Radboud University Nijmegen

Faculty of Science

Implementation of LGAD gain reduction into the Allpix Squared framework

Implementation of gain reduction due to screening of the electric field in Low Gain Avalance Diodes into the Allpix Squared simulation framework

Thesis BSc Mathematics & Physics and Astronomy

Author:
Femke de Wit

Supervisor:
Dr. Frank Filthaut
Radboud Universiteit

Second supervisor:
Dr. Marcos Fernandez Garcia
Universidad de Cantabria

in collaboration with the CERN SSD group

July 14, 2023

Abstract

For the new upgrades for the experiments on the Large Hadron Collider at CERN, Low Gain Avalanche Diodes (LGADs) will be used. These silicon detectors allow for precise timing measurements because they are thin and they have an internal gain. It is of essence to know what the gain of the device is to interpret the signal. However, recent research has shown that the gain is dependent upon the charge carrier density in the so-called gain layer of the device. A parametrization of this physical phenomenon has been put forward. The goal of this thesis was to implement this parametrization of LGAD charge carrier dependent gain reduction in the simulation framework Allpix Squared and compare the results both to the original publication of the parametrization and to gain experiments we did at the laboratory of the Solid State Detectors group of the Experimental Physics department of CERN. To this end, first a simpler way to model the electric field of an LGAD was introduced in Allpix Squared. The gain reduction itself was implemented in two different ways using different functions. One function reduces the electric field in the gain layer by a constant perturbation, which results in less impact ionization and thus less gain. The other function reduces the gain directly by a power law derived in the original publication. The implementations in Allpix Squared reproduced the results from this publication well. The function that directly reduces the gain by a power law is especially very accurate. When Allpix Squared simulation is compared to TCAD simulation of the same device, it fails to reproduce the contribution to gain from holes. Measurement of devices, simulated with both packages, confirm that hole multiplication should not be discarded.

Contents

Definitions, symbols and abbreviations

Definitions

Algorithm
The calculation of gain in the propagation module. There are two algorithms. The first one is the accumulated gain algorithm. It was later superseded and a new version was introduced, which was the probability based algorithm. It should be noted that these algorithms were not created during this internship, but by the maintainers of Allpix Squared [1].

Electric field type
Allpix Squared provides several options for the shape of the electric field in the detector due to bias voltage. These include for example a linear field or a parabolic field. In this work, a new type is proposed, called gain layer field. This gives an approximation of an electric field of a Low Gain Avalanche Diode.

Function
A separate file in the Allpix Squared framework that performs the calculation of a single physical quantity, such as the mobility or multiplication factor. A propagation module can call upon this function. In this work, two new functions were added, namely the GainReduction function and the ElectricFieldScreening function.

Implementation
The additions of the two gain reduction functions and a new electric field type created in this thesis.

Model
A model is essentially an equation with data-fitted coefficients describing a complex physical quantity in a relatively simple way in Allpix Squared. There are often several models available for the calculation of physical quantities which depend on the data set used to fit coefficients. Functions usually contain multiple models. The user can choose which model the function should use for calculations. The functions GainReduction and ElectricFieldScreening contain each only one model.

Module
A part of the simulation chain of Allpix Squared. A single simulation is split up into different modules, each performing a part of the process, such as the calculation of the electric field, the deposition of charge carriers, the propagation of charge and so on. Usually, there are several modules available to perform one task. The user should choose which version to use. The modules can only communicate using messages.

Symbols

G_{acc}
Accumulated gain. Gain calculated in the accumulated gain algorithm for every charge carrier group. As a charge group propagates, it accumulates a gain from which the amount of new charge carriers is calculated and it ends up with a final accumulated gain.

G_0
Unreduced gain. Gain in a simulation or experiment if there were no gain reduction present.

$\bar{G}$
Average gain. A quantity used in the parametrization in [2] to include the negative feedback loop described at the end of Section 2.3.

G_{pred}
Predicted gain. The result of a quick calculation done by the GainReduction and ElectricFieldScreening functions. The gain is calculated as a final accumulated gain of an electron propagating through the gain layer. The quantity is used in the implementation in Allpix Squared as the average gain from [2].

G_{red}
Reduced gain. The reduced gain as a result of Equation 5.

Abbreviations

FWHM
Full Width Half Maximum. For a gaussian curve this is the distance between the two points at half of the maximum amplitude.

HPK
Hamamatsu Photons K.K. A company from Japan which produces amongst others silicon detectors. The detectors used in this study are all from this company.

LGAD
Low Gain Avalanche Diode. A silicon detector with an internal gain layer near the pn-junction.

PIN
P-doped, Intrinsic, N-doped. A detector comparable to a Low Gain Avalanche Diode and from the same wafer but without the gain layer. It is used in this thesis to calculate the gain of the corresponding LGAD.

TCAD
Technology Computer-Aided Design. A simulation technique based on solving complex systems analytically.

TCT
Transient Current Technique. A measurement technique in which a signal is created by the current induced on electrodes due to the movement of free charge carriers.

1 Introduction

The Conseil Européen pour la Recherche Nucléaire, or CERN, is the most pronounced laboratory for the field of high energy physics in the world. It is home to the Large Hadron Collider (LHC), a particle accelerator with a circumference of 27 kilometers. Particles, usually protons, accelerate in the LHC to nearly the speed of light. Two beams go in opposite direction and collide in each of the four experiments that are on the LHC. During this collision, new particles are formed and scattered, and then measured by the experiments. The four experiments are ALICE, LHCb, CMS and ATLAS. The ALICE experiment is specialized in studying strongly interacting matter at very high energy densities to investigate quark-gluon plasma [3]. LHCb was built to examine and understand the subtle differences between interactions of antimatter and matter by studying the beauty quark [4]. ATLAS and CMS are both multipurpose detectors [5] [6]. They implement different technologies but are designed to accurately measure the same phenomena. As the LHC is the only accelerator that can reach these high energies, it is important to have two experiments can verify each other's discoveries.

ATLAS and CMS both are constituted by specialized subdetectors: the tracker, the calorimeters, the magnets and the muon chambers. The design and position of these components are different for the two experiments. Figure 1 shows where these four components are located in CMS. Particles created in the collisions first cross the tracker. The tracker consists of two parts, an inner tracker with pixel detectors and an outer tracker with strip detectors. Pixels provide intrinsic 3D resolution. So-called stereomodules of strips can provide 3D information with a different precision. The particle track is reconstructed from this information. After passing the tracker, particles cross the calorimeter. This also consists of two parts. The inner part is the electromagnetic calorimeter and this measures the energy of photons and electrons. The outer part is the hadron calorimeter which measures the energies of hadrons such as protons and neutrons. In CMS, the next part is the magnet (in ATLAS the magnet is situated after the tracker). In the CMS experiment, this magnet is in the shape of a solenoid and creates a magnetic field in entire experiment that bends the tracks of the particles. How much a particle track is bent in the magnetic field determines its momentum. Outside of the magnets are the muon chambers. Most particles are stopped in the calorimeters, but neutrinos and muons pass and reach the muon chambers, where the muons are detected.

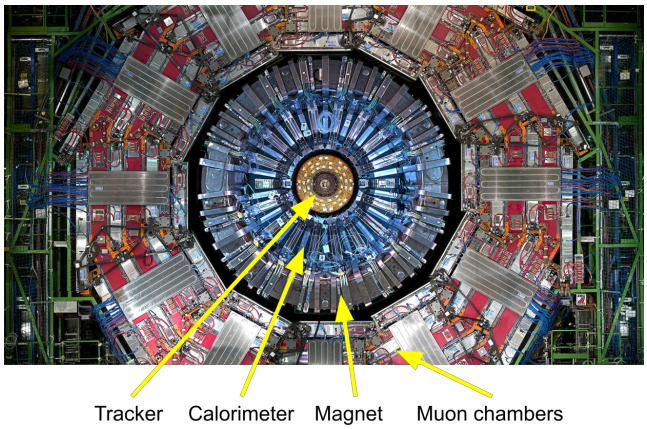

Figure 1: A cross section of the CMS experiment displaying the position of the tracker, calorimeters, magnet and muon chambers [6].

The LHC will undergo an upgrade to the High Luminosity LHC (HL-LHC), starting operation around 2029. In this upgrade, the number of collisions will increase by a factor ten. Up to now, no timing measurements are done in CMS and ATLAS. Track reconstruction is done only from information on the spatial coordinates of track points (3D tracking). One of the improvements of the upgrade is that timing information will be included. For the ATLAS experiment, timing measurements will be done by the High Granularity Timing Detector (HGTD). For CMS, timing measurements will be done by the MIP Timing Detector (MTD). This will entail avalanche photomultipliers between the tracker and calorimeter in the barrel and Low Gain Avalanche Diodes (LGADs) at the end caps. LGADs are also used in the HGTD for ATLAS. LGADs have a very good timing precision. Accurate timing measurements are an essential part of the HL-LHC upgrade, because there will be more tracks from the collisions and thus better track reconstruction is needed. Good timing precision enables better track reconstruction because track points cannot be distinguished only in space, but also in time. This is called 4D tracking. These LGADs and how to correctly model their properties in a simulation framework called Allpix Squared is the main focus of this thesis. First, in order to understand how the LGAD works, a background on silicon detectors is given.

2 Theoretical background on silicon detectors

2.1 Semiconductors

The large majority of tracking detectors in high energy physics are made of silicon. Silicon has four electrons in the outer shell. These valence electrons establish valence bonds between silicon atoms to form a lattice structure. It is sometimes possible for electrons to escape from the lattice and turn into conduction electrons, which can freely move around in the material. The minimum amount of energy needed for an electron to escape is the energy gap. This energy gap, or band gap, is a range of energies in which no energy states exist for electrons. A valence electron has an energy below this band gap, in the so-called valence band. A conduction electron has obtained enough energy to overcome this energy gap and has an energy in the so-called conduction band. In the case of insulators, this gap is too large to overcome and electrons are fixed in the lattice. In the case of conductors, this energy gap is (almost) absent. Little energy is required to generate conduction electrons. Silicon is a semiconductor. Semiconductors have a small band gap of only a couple of electron-volts. The band gap of silicon is for example around 1.12 eV at room temperature [7]. With thermal excitation or some other energy source, electrons can be freed from the lattice. When an electron is freed, a hole remains. This hole is the absence of a valence electron in the lattice. Together they form an electron-hole pair (eh-pair).

2.2 pn-junctions

When a piece of silicon contains exclusively silicon atoms, it is called intrinsic silicon. In the case of detectors however, other types of atoms are added into the silicon lattice. This is called doping. When silicon is doped with Phosphorus, which has five valence electrons, the silicon is n-doped. The Phosphorus in the lattice has an extra electron compared to silicon which cannot create a valence bond and therefore very easily becomes a free electron. When silicon is doped with Boron or Aluminium (less common), which have only three valence electrons, the silicon is p-doped. Because the Boron (or Aluminium) can only form three bonds, a hole remains. A hole can be considered a charge carrier much like a free electron but with opposite charge. Holes can also move around the material, as shown in Figure 2. When silicon is n-doped, there is an excess of electrons and when

the silicon is p-doped, there is an excess of holes. In any case, the material remains charge neutral.

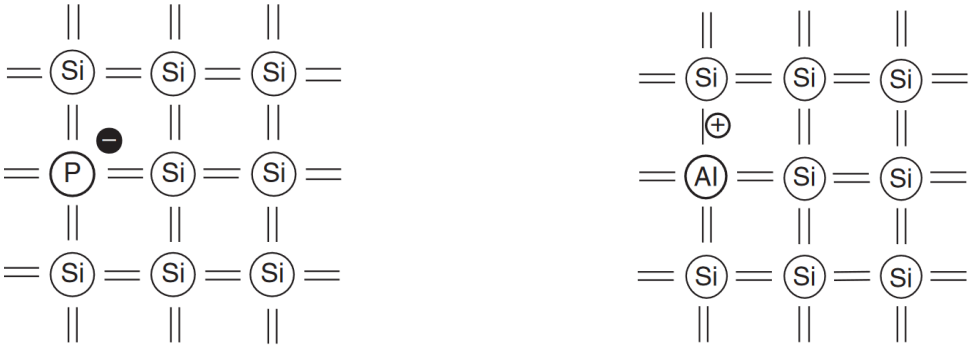

(a) Donor (b) Acceptor

Figure 2: Doping of silicon with a donor and an acceptor creating a free electron and a hole [8].

A pn-junction consists of n-doped silicon in contact with p-doped silicon. At higher temperatures (for silicon, room temperature is enough), electrons from the n-doped silicon can diffuse partly into the p-doped silicon and holes from the p-doped silicon can diffuse partly into the n-doped silicon. When this happens, the diffused electrons originating from the n-doped silicon can recombine with the holes in the p-type silicon. And conversely, diffused holes originating from p-doped silicon can recombine with electrons in the n-type silicon. This creates a region close to the pn-junction with very little excess charge carriers. This is called the depletion region. The charge density is no longer neutral in the depletion region. In the p-type silicon, excess electrons recombined with the holes, which results in a negative space charge. In the n-type silicon, it is exactly the other way around forming a positive space charge. The space charge creates an electric field over the pn-junction. This electric field created from diffusion in turn hinders the diffusion of the charge carriers over the pn-junction.

The size of the depletion region can be manipulated by applying an external bias voltage. Because of this bias voltage, the charge carriers do not only move randomly because of diffusion, but can also have directed movement, called drift, towards the corresponding electrode. When the p-type silicon is attached to the cathode and the n-type silicon to the anode, the holes in the p-type propagate towards the anode and the electrons move in opposite direction, see Figure 3a. This is called a forward bias. The depletion region is decreased, decreasing the barrier electric field and current can flow over the pn-junction. When the anode and cathode are attached in the opposite way, the charge carriers are forced in the other direction, creating a larger depletion region, thus leaving behind a larger region of space charge and a larger electric field. No current due to majority charge carriers can flow through. Figure 3b depicts such a reverse bias.

In silicon sensors, the properties of the depletion region are exploited. For silicon sensors, a reverse bias is applied to (fully) deplete the sensor. Usually, one of the two sides is much larger than the other. In case of full depletion, the silicon contains no free charge carriers. A linear electric field is created by a uniform space charge distribution. When a particle with enough energy transverses the sensor, silicon atoms are ionized creating eh-pairs. The eh-pairs propagate in the electric field to

their respective electrode. The induced current that these propagating electron-hole pairs produce on the electrodes is read out by the front-end electronics attached to the sensor. The precise 3D location where the particle crossed the sensor can be deduced by pixelating the detector. The time the particle crossed can be deduced by comparing the signal to an external clock. This is the basic workings of silicon detectors [7].

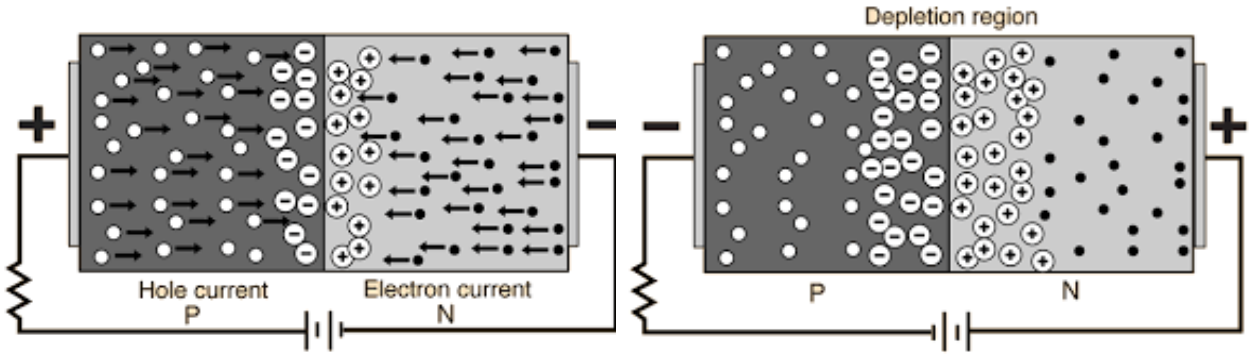

(a) Forward bias (b) Reverse bias

Figure 3: pn-junction with a forward an reverse bias applied. In the case of forward bias, electrons and holes can cross the pn-junction to create a current and reduce the size of the depletion region. In case of a reverse bias, the electrons and holes are pulled away, creating a larger depletion region and thus a larger electric field that acts as a barrier for current. No current of majority charge carriers can flow under a reverse bias unless the bias is so high that the diode is in breakdown [9].

2.3 LGADs

There are many different types of silicon detectors. Some can accurately measure the location at which a particle crossed and other types perform well on timing measurements. In the experiments on the LHC, a large amount of silicon detectors with high spatial accuracy form the tracking systems. A signal is induced in these detectors when a particle from the collision traverses the sensor. From the locations of the signals, particle tracks starting from the interaction point can be reconstructed. However, in the case of many particles this reconstruction process can be difficult. This is improved by adding detectors with good timing accuracy to the setup. By including a time component, it easier to distinguish between different tracks. An example of a detector with good timing precision is the LGAD mentioned in Section 1. LGADs are relatively thin detectors with, as the name suggests, an internal gain layer. Because of these two characteristics, the rise time of the signal is very small. This sharp, peaked signal provides a good timing resolution.

LGADs are usually built on a p-bulk. In that p-bulk, a p^+-implant is situated close to the pn-junction. The p^+-implant is only a few microns thick. In this p^+-implant, a very high electric field forms as can be seen in Figure 4. In the high field, the electrons moving towards the cathode are sped up. The electrons obtain so much drift velocity that they can ionize silicon and create new eh-pairs. This is called impact ionization. The secondaries from impact ionization can in turn ionize silicon again. This is known as the avalanche effect. This avalanche creates extra charge carriers and an extra induced signal, a gain. Experimentally, the gain of an LGAD is often the induced charge of the LGAD divided by the induced charge of a PIN (an LGAD without the gain layer). Another way the gain is calculated experimentally is by injecting red light from the back and differentiating between the electron and hole contribution of the signal. In the case of backside

injection with red light, only the primary electrons contribute to the first peak of the signal and only the secondary holes contribute to the tail of the signal, as shown in Figure 5. By identifying these two parts and dividing the induced charge of the secondary holes by the induced charge of the primary electrons, the gain is estimated. In simulations, the term "gain of a charge carrier group" is sometimes used. In this case, the gain usually describes the amount of secondary eh-pairs produced by this group in a certain step through the sensor. These secondaries include also any eh-pairs produced by the secondaries themselves.

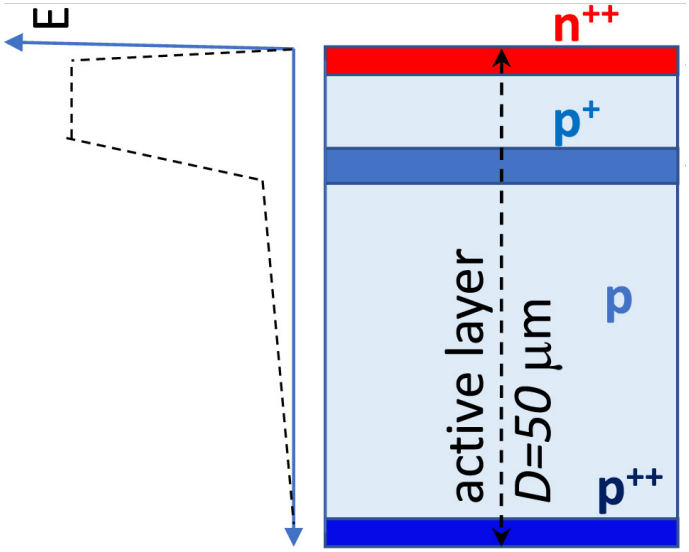

Figure 4: Example electric field shape of an LGAD. The figure is not to scale. The pn-junction is located between the n^{++}-implant in red and the gap below it. The thickness of the detector is 50 µm and the gap is in the order of a few microns thick. The electric field is very high in the gain layer compared to the bulk [2].

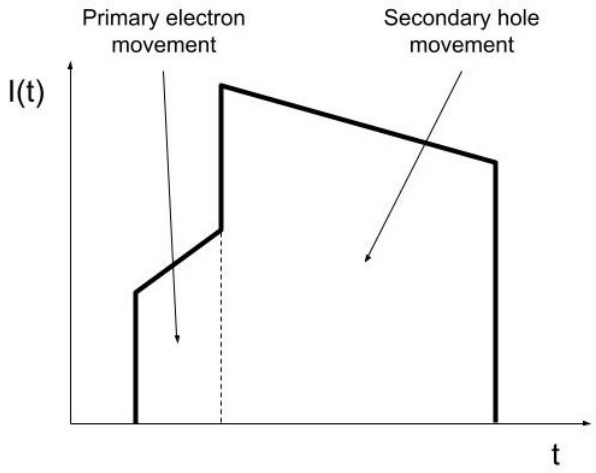

Figure 5: Induced current signal of backside red injection in an LGAD

Impact ionization is a statistical process. It can be described quantitatively by defining a mean free path λ as the mean distance between two events of impact ionization [10]. The gain a charge carrier obtains whilst propagating through a sensor is then given by

$$G = e^{\alpha(E,T)l}, \tag{1}$$

where α is the impact ionization coefficient and $\alpha = 1/\lambda$. α is a function of the local electric field E and the temperature T. It also depends on whether the carrier is an electron or a hole. l is the distance traveled in the field E. In case of a non-uniform electric field, this formula can be broken up into paths of size Δl where the electric field is assumed constant,

$$G = \prod e^{\alpha(E_\mathrm{i},T)\Delta l_\mathrm{i}}. \tag{2}$$

The impact ionization coefficient α follows the Chynoweth law [11]. For the Chynoweth law, various parametrizations of the coefficients are available. For example, the Overstraeten deMan model [12] is given as

$$\alpha(E) = a_0 e^{-\frac{E_\mathrm{C}}{E}}, \tag{3}$$

where a_0 and E_C are coefficients and depends again on the carrier type. Most parametrizations of the impact ionization coefficient have a similar form. It is important to note that the gain is effectively a function of a double exponent of the inverse of the electric field. Therefore, it is a very sensitive parameter to the electrical geometry of a detector.

Research conducted at the host group where I did this thesis has shown that the gain of an LGAD is dependent on the eh-pair density in the sensor [13]. Because the gain layer is very thin and a lot of charge is created there, this charge can disturb the external electric field. The interactions of the charges in the gain layer is a complex physical process. A first order approximation of this process was given by Gregor Kramberger et al. in [2]. Charge created by gain consists of eh-pairs, where the electrons and holes move in opposite direction. The separation of the multiplied carriers induces a small dynamic internal electric field that opposes the external electric field produced by the bias voltage (see Figure 6). This perturbs the external electric field. Because the impact ionization is sensitive to the electric field, the impact ionization magnitude decreases and therefore also the gain decreases. Thus, when the density of eh-pairs in the gain layer is very high, either due to a very high gain or because of a very small deposition volume, a lower gain than expected is measured. This is a negative feedback loop. The higher the gain, the more gain reduction and thus the lower the gain until an equilibrium reduced gain is reached.

2.3.1 One dimensional parametrization of gain reduction

In [2], a parametrization of this phenomenon of gain reduction is made in the case of infrared laser deposition. In this approximation, the secondary electrons and holes are assumed to form a parallel plate capacitor, charged to the amount of secondary eh-pairs present The distance between plates is approximated to be the same as the thickness of the gain layer. A picture of this is shown in Figure 6.

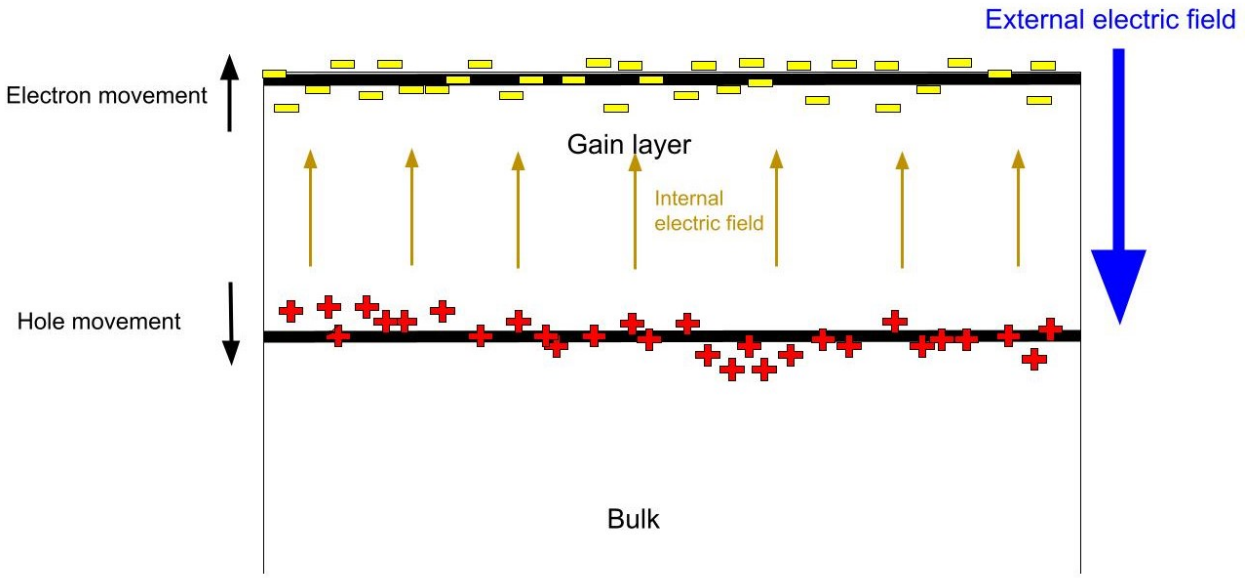

Figure 6: The parallel plate assumption is based on the secondary charges moving in opposite direction creating a parallel plate with an internal electric field in the opposite direction of the external electric field from the bias voltage.

This internal electric field is given by [2]:

$$\Delta E = \frac{e_0}{\epsilon\epsilon_0} d_{\mathrm{gl}} (\bar{G} - 1) n_{\mathrm{eh}}, \tag{4}$$

where d_{gl} is the thickness of the gain layer and n_{eh} is the volumetric density of eh-pairs deposited in the sensor by the laser. The average gain $\bar{G}$ is taken as the average gain from the negative feedback loop described in Section 2.3. Thus, $(\bar{G} - 1) d_{\mathrm{gl}} n_{\mathrm{eh}}$ gives the surface charge density of the parallel plate. Using Chynoweth's parametrization of the impact ionization coefficient α and a first order Taylor approximation on $\Delta E << E$, a formula is obtained for the reduction of the gain.

$$G_{\mathrm{red}} = G_0^{1 - b n_{\mathrm{eh}}}, \qquad b = \frac{E_{\mathrm{C}}}{E^2} \frac{d_{\mathrm{gl}} e_0 (\bar{G} - 1) n_{\mathrm{eh}}}{\epsilon\epsilon_0}, \tag{5}$$

where G_{red} is the reduced gain, G_0 is the original gain without gain reduction, E is the external electric field and E_{C} is the parameter from the Overstraeten deMan model for the impact ionization coefficient. A derivation of Equation 5 can be found in [2].

3 The Allpix Squared framework

The work done in this thesis is implemented into the framework Allpix Squared [1]. Allpix Squared is a Monte Carlo based C++ program designed to be a user friendly simulation tool to simulate semiconductor detector setups. It was first released six years ago and since then over 50 researchers have contributed to the code. It uses Geant4 [14], ROOT [15] and Eigen [16] to model any detector setup. Geant4 is used mostly for calculating interaction between the source and the detector material. ROOT is used for histogramming and analysis. Eigen is used as a mathematical tool.

Allpix Squared can simulate many types of sources (ionizing particle beams, lasers, radioactive sources and more) which can generate signals in an arbitrarily large amount of detectors that can each be custom designed. The user can for example define the location, size, support material, electric field, and weighting field [17] of each detector. Also the way electron-hole pairs are transported through the sensor and the way the signal is read out and digitized can all be customized by the user. In this section, more information will be given on the workings of this program. Specifically the way in which gain is implemented is highlighted.

3.1 Structure

One of the big advantages of Allpix Squared is its modular structure. All parts in the simulation chain are decoupled into modules. Each module performs a part of the simulation. This can for example be propagating deposited charges through a specific sensor. The modules can only interact with each other through a messengers system. The messages carry objects. For example, there is a DepositedChargeMessage, which contains DepositedCharge objects.

For a typical simulation, first the geometry is built. This means that all detectors are placed at the right coordinates and fields are calculated for every detector. For this, the GeometryBuilderGeant4 module in combination with the ElectricFieldReader module could, for example, be chosen. After that, the deposition is simulated. This could for example be done with the DepositionGeant4 module or with the DepositionLaser module. Then, deposited charges are propagated through the sensor material. There are many modules available to do this, like the TransientPropagation module or the GenericPropagation module. After that, the propagated charges are transferred to the readout chip using for example the SimpleTransfer module or the PulseTransfer module. Lastly, they can be digitized with for example the DefaultDigitizer module. Figure 7 shows an example of a typical simulation for three detectors which are all adjusted individually. The general structure of Allpix Squared is illustrated in Figure 8.

Throughout the simulation, modules can call onto several functions. Each function performs a calculation for a particular physical quantity. There are usually several models describing this quantity. These are called the physics models in Allpix Squared. In this thesis, a function refers to a group of physics models that calculate the same physical quantity. For example, there are various physics models for calculating the Mobility.

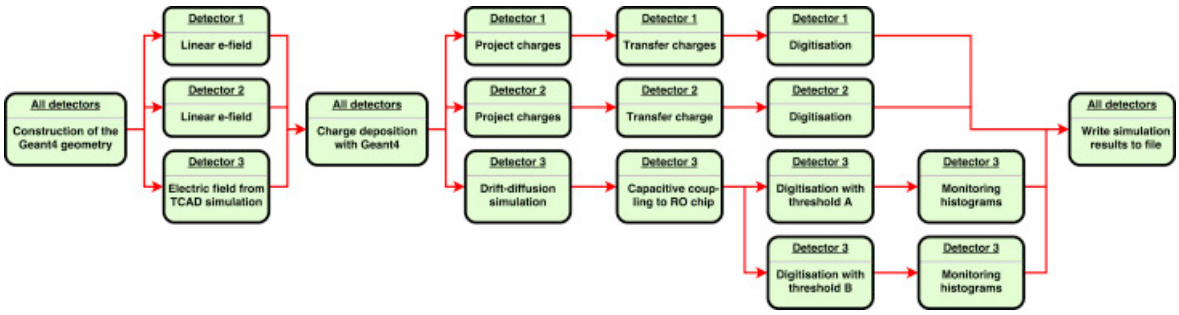

Figure 7: An example of a simulation with Allpix Squared. Three detectors are simulated for which the deposited charge is processed each in a different way [1].

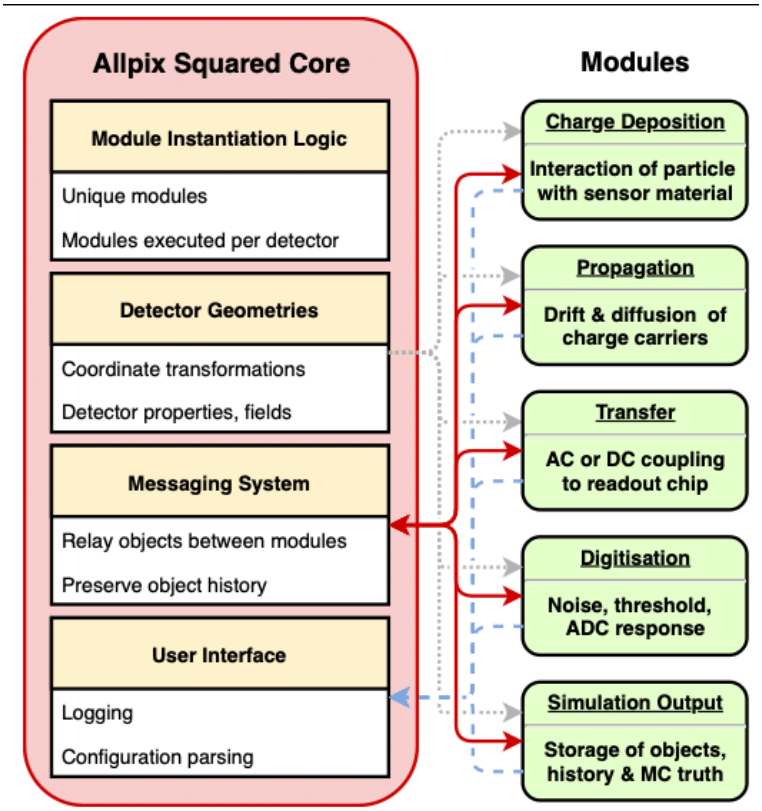

Figure 8: Basic structure of Allpix Squared. The input and output of the modules are passed to one another through the messaging system [18].

In the drift-diffusion model, the mobility μ is the proportionality constant between the drift velocity v_{drift} and the electric field E; $v_{\text{drift}} = \mu E$. Physically, it is expected that the acceleration is proportional to the electric field, not the velocity. However, drift velocity is a more complex concept. It describes the average velocity of charge carriers in a lattice, taking into account the acceleration in the electric field as well as the deceleration due to collisions with the lattice. Because of this, the mobility is dependent on quantities such as the effective mass and average time between collisions. Moving away from such averages and considering the real microscopic behaviour of the charge carriers in the lattice and field would be too computationally expensive. Thus the drift-diffusion model is used in Allpix Squared. This means that the drift velocity is used to describe charge carrier velocity. Relatively simple phenomenological models are used for the mobility.

In any propagation module, the Mobility function can be called to calculate the mobility as a function of the electric field value that the propagation module provides. There are many different models that the Mobility function can use to calculate the mobility, such as the widely used Jacoboni-Canali model [19] or the Hamburg model [20]. Models are essentially equations with data-fitted temperature-dependent coefficients. Different models can use different equations but it is also possible that they only differ in the temperature dependence of the coefficients. Which model is best for a simulation depends on the simulated device and can be set by the user.

The user specifies the setup of a simulation through the use of configuration files. These are text files that can be read by the program. There is a main configuration file, containing a list

of all used modules and the parameters per module. It is also specified per module which physics models are used. Then, there is a separate detector configuration file that contains the information on all the detectors such as the position and the detector model. Lastly, there are detector model configuration files. These files contain the detector types which need to be specified in the detector configuration file. There are already many of these detector model configuration files provided by Allpix Squared, but the user can also create a custom one.

3.2 Multiplication in Allpix Squared

In the propagation modules, deposited charge messages are used as input. A deposited charge message contains a list of all deposited charge groups and information on each charge group such as a time stamp, position and charge. The propagation module propagates the charge groups consecutively and in steps. This means that the charge groups cannot interact with each other. At every step of the propagation of a charge group, physics functions can be called upon. After propagating all charges, the propagation module generates an output message containing all charge groups and additional information such as the propagation time, the final position and the state. This propagated charge message can later be used again by another module, similar to how the deposited charge message was used by the propagation module. The two propagation modules considered in this thesis are the TransientPropagation and GenericPropagation. They work quite similarly, as they both calculate the track of charge carriers by drift in the electric field and diffusion. Their main difference is that GenericPropagation does not keep track of the induced charge, making it a more lightweight module compared to TransientPropagation.

The addition of gain in the TransientPropagation and GenericPropagation is to be part of the next Allpix Squared official release. At first, an algorithm based on the accumulated gain of charge carrier groups was used. In the process of this thesis, a new version of the algorithm was created which was probability based.

Both versions make use of the ImpactIonization function, containing many physics models for the impact ionization coefficient α. Just like for mobility, the microscopic physics behind impact ionization is complex. It describes the exchange of kinetic energy from a charge carrier to a valence electron in a scattering event. In Allpix Squared, this is simplified by considering the impact ionization coefficients from the drift-diffusion model. The ImpactIonization function gives the local gain (or multiplication factor) as a function of the local electric field, step length and carrier type. The function calculated the gain using Equations 1 and 3 and the models are the models existing for alpha, such as the Massey model [21] or the Overstraeten deMan model [12].

In the accumulated gain algorithm, every charge group starts out with an accumulated gain of $G = 1$. At every step, this accumulated gain is multiplied by the local gain of that step, calculated by the ImpactIonization function as the multiplication factor. The accumulated gain is calculated similar to Equation 2. At every step, the accumulated gain is increased according to

$$G_{\text{acc}} = G_{\text{local}}(E, \Delta l) G_{\text{previous}}. \tag{6}$$

Here, E is the absolute value of the electric field vector, Δl is the step length. Also the carrier type is taken into account. An example of the difference between the local gain and the accumulated gain is depicted in Figure 9. When the accumulated gain crosses an integer threshold during propagation, a new charge carrier group of opposite type is generated. There are no new charge carriers of the same type created, but instead, the module keeps track of the gain and the final

charge of the charge group is taken to be $G_{\text{acc,final}}Q$, where Q is the charge of the group before propagation. For TransientPropagation, the induced charge is calculated from GQ at every step. The reason to only generate new charges when an integer value of the gain is crossed, is to ensure that the charges remain discreet. However, because of this, the total amount of created charge is rounded down to the nearest integer and because of that also the total amount of induced charge is reduced. Take for example a case in which all electrons end up with a final accumulated gain of 2.1. This means that all electrons have created one extra eh-pair. If the electrons would have ended up with a total accumulated gain of 2.9, there would also have been only one new eh-pair per electron. However, impact ionization is a probabilistic process and not deterministic, meaning that more charge carriers should be created when the gain is 2.9 compared to when it is 2.1.

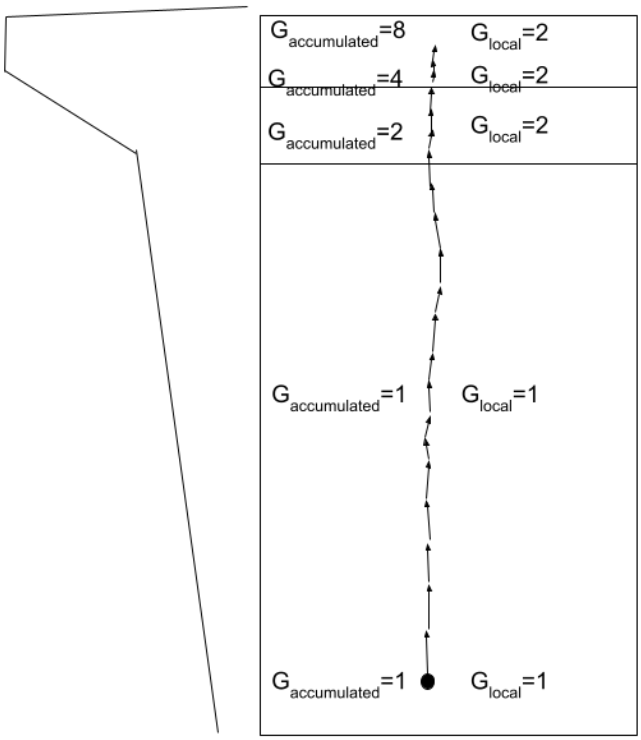

Figure 9: A depiction of the two definitions of accumulated gain and local gain. The local gain is calculated from the local electric field and the step size. It is recalculated at each step whereas the accumulated gain is the product of all previously calculated local gains.

The new algorithm, the probability based algorithm, does include this statistical aspect of impact ionization. This approach relies only on the local gain at every step. For every step, the local gain of the charge group is again calculated by the ImpactIonization function. From this local gain, the amount of secondary charge carriers n is calculated for every charge in every group. This is done by taking a random sample of a geometric distribution with the mean equal to the local gain. The method to draw randomly from the geometric distribution is called the inversion method and is further explained in Appendix B.

Summing over all the secondaries produced by all the charges within a group gives the total amount of secondaries created by the charge group in that step. The total charge of the charge group is

increased by this amount, and the new charges of opposite type are created and propagated. The final gain of a charge carrier group is the amount of charges in the group divided by the amount of charge before propagation. In case the size of the charge groups is set to 1, the final distribution of the gain of the charge carrier groups follows a geometric distribution reflecting the distribution from which the secondaries are drawn. In TransientPropagation, the induced charge is now calculated from Q, instead of GQ like for the accumulated gain algorithm, because the charge of the group is increased during propagation.

The gain reduction implementations discussed in this thesis are tested on both these algorithms. It should be noted that the aim of this thesis is not to investigate the workings of any gain algorithm, but rather the behavior of the gain reduction implementation as independently of the gain algorithm as possible.

4 Additions to the Allpix Squared framework

In order to implement gain reduction phenomena into Allpix Squared, three additional parts have been added in this work. First is the option for the user to set the electric field type to the approximate typical electric field of an LGAD. The other two additions are two different functions containing physics models to simulate gain reduction. One version simulates gain reduction by reducing the final gain of every charge group according to Equation 5. This is the GainReduction function. The other version simulates the screening of the electric field according to Equation 4, resulting also in a reduced gain. This is the ElectricFieldScreening function. They should simulate the same effect but each in a different way. After a brief explanation of the geometry, more will be explained on these implementations in Section 4.1 and Section 4.2.

4.1 Gain layer electric field implementation

Allpix Squared does not determine the electric field from a doping concentration given by the user. Instead, it requires the user to specify explicitly the shape of the electric field together with some necessary parameters. The field types that were already implemented in Allpix Squared are constant, linear, parabolic, custom and mesh. Constant fields are not very physical, but allow for a simple model in order to test other parts of the framework. Linear fields are good approximations in the case of a diode-like detector. In the case of irradiated detectors, parabolic fields are a good approximation. The custom field type lets the user choose the shape of the electric field themselves. When a mesh field type is chosen, the user must give a file containing a discretized map of the electric field. This can be for example the result of a TCAD simulation. All field types except for custom and mesh are one dimensional.

Although the typical shape of the electric field of an LGAD could be obtained by using the custom or the mesh field type, there used to be no general option to apply such a field to a detector. Therefore, as part of this work, this option was added to the Allpix Squared framework. The new type of field is called "gain layer". The shape of this electric field type is depicted in Figure 10 together with the doping profile. It is one dimensional.

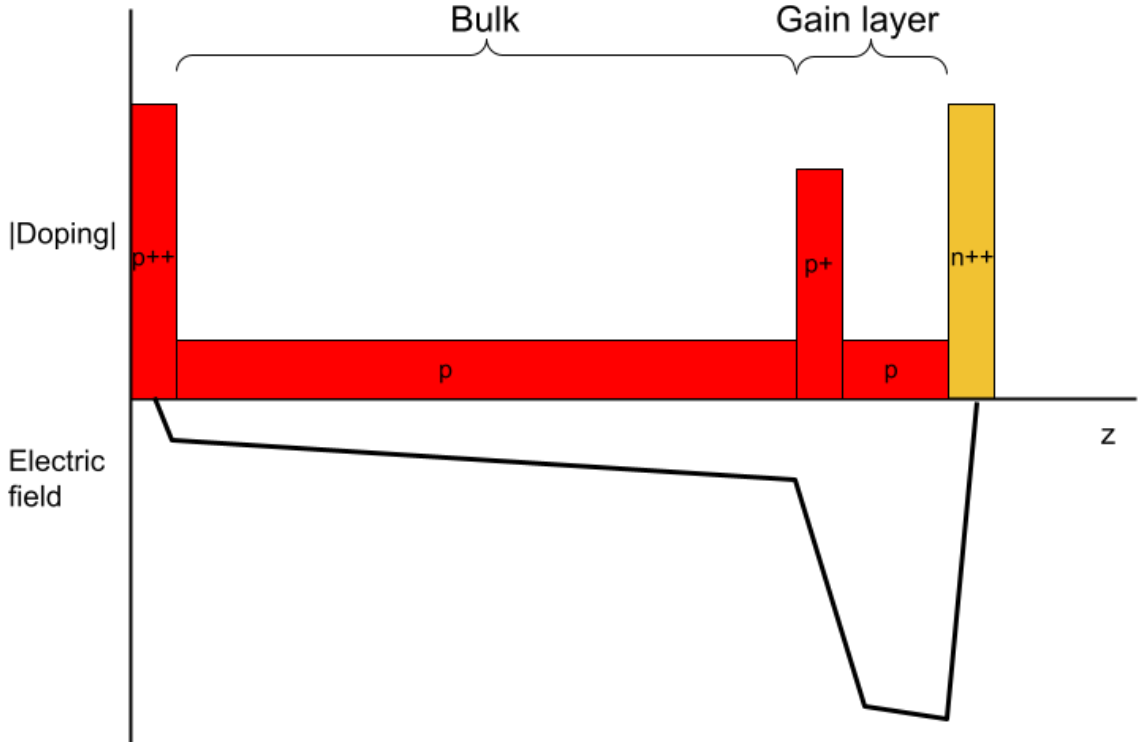

Figure 10: Box model of the doping. The backside p^{++}-implant (ohmic contact), p-bulk, p^{+}-implant, gap and frontside n^{++}-implant are all considered to have a constant effective doping. The corresponding electric field approximation in case of overdepletion is also shown. Both the doping and electric field are not to scale.

It takes the following input parameters from the user:

- Bias voltage V_{bias} (required): the external voltage applied to the detector
- Depletion voltage V_{depl} (defaults to 5 V): the voltage needed to deplete the bulk, which has a thickness of sensor without the gain layer
- Gain layer voltage V_{gl} (defaults to 50 V): the voltage needed to deplete the entire gain layer, including gap
- Implant thickness d_{imp} (defaults to 1 µm): the thickness of the p^{+} implant
- Gap thickness d_{gap} (defaults to 1 µm): the thickness of the gap between the n^{++}-implant and the p^{+}-implant

The gain layer voltage and the depletion voltage can be obtained by measurements. The implant and gap thickness (as well as the doping) of the gain layer and gap are often not revealed by manufacturer of the detector, but they are necessary parameters to determine the electric field. These values need to be determined from experiments or carefully estimated by the user. The overall thickness of the bulk is given separately in the detector model configuration file.

Generally, to deplete a sensor until depth z from the pn-junction (thus $z = 0$ at the pn-junction) with constant effective doping N_{eff}, the voltage required is [10]

$$V(z) = \frac{q_0}{2\epsilon\epsilon_0}|N_{\text{eff}}|(z-d)^2. \tag{7}$$

Therefore, the depletion voltage of a sensor of thickness d and constant effective doping N is given by

$$V_{\text{depl}} = \frac{q_0}{2\epsilon\epsilon_0}|N_{\text{eff}}|d^2. \tag{8}$$

Taking the derivative with respect to z of equation 7, we obtain a linear function for the electric field

$$E(z) = \frac{q_0}{\epsilon\epsilon_0}|N_{\text{eff}}|(z-d). \tag{9}$$

Solving equation 8 for $|N_{\text{eff}}|$ and plugging this into equation 9, a relationship between the electric field and the depletion voltage and thickness is obtained:

$$E(z) = \frac{2V_{\text{depl}}}{d^2}(z-d). \tag{10}$$

This is the one dimensional linear field approximation for a simple diode. For an LGAD, the same principle is applied. Instead of one box of constant doping, there are now multiple constant doping "boxes" (see Figure 10). The electric field is calculated using Equation 10 for each box. Depletion starts from the pn-junction between the n^{++}-implant and the lightly p-doped gap. In this approximation, depletion of the frontside n^{++}-implant and backside p^{++}-implant are neglected. This is consistent with the other approximate field types in Allpix Squared, which also do not include the n^{++}- and p^{++}-implants. The following part will describe in more technical detail how the electric field is calculated.

4.1.1 Overdepletion

As the voltage is the integral over distance of the electric field, the area under the electric field function can be split up into multiple voltages. Figure 11 shows the definitions of the voltages used in this model in the case of overdepletion. If the bias voltage is not high enough to deplete the entire detector, it is called underdepletion. This can be such that only the bulk is underdepleted, but also such that also the implant or even also the gap is underdepleted. In these cases, we consider effective thicknesses and effective voltages. They are depicted in Figure 12.

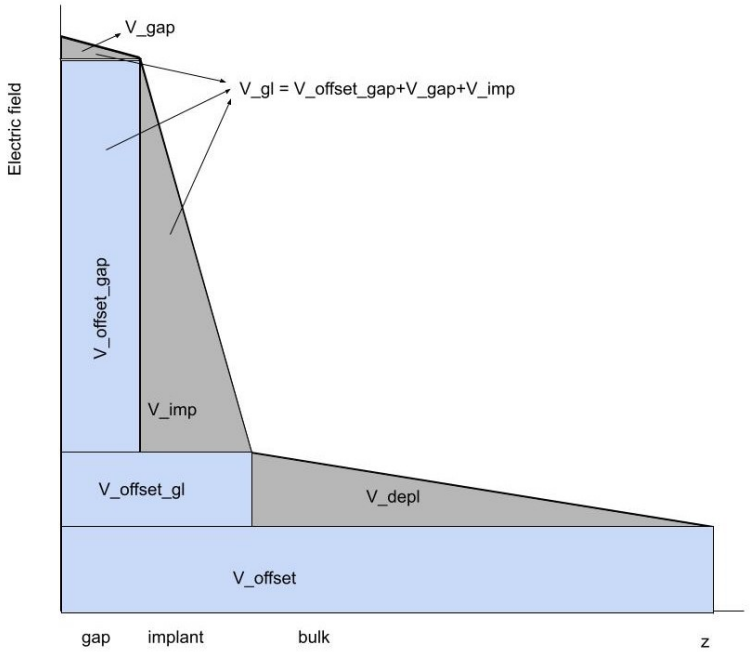

Figure 11: Definition of all the types of voltages in case of overdepletion. Note that the coordinate system is shifted with respect to Figure 10. The z-axis is rotated and the absolute value of the electric field is considered.

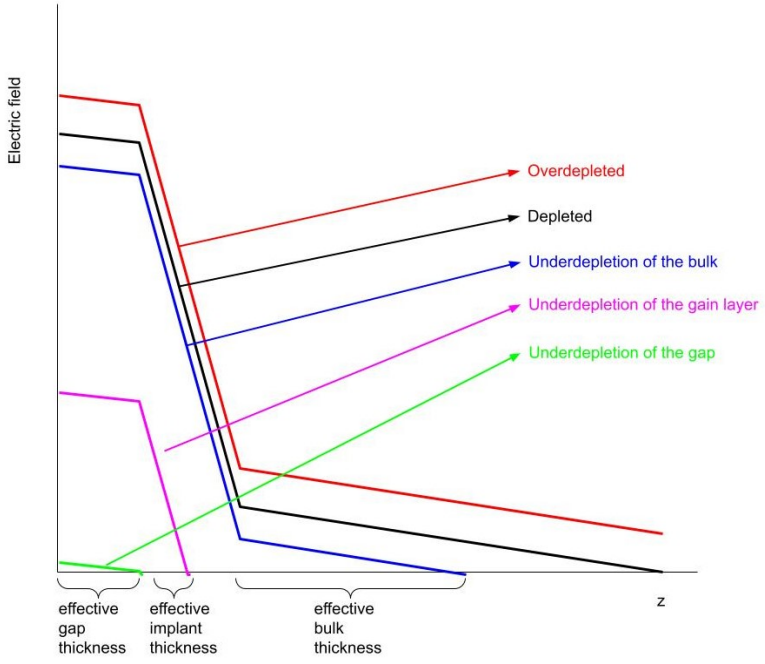

Figure 12: Shape of the electric for the different cases of depletion. In case of underdepletion, an effective thickness can be defined.

The following part assumes overdepletion ($V_{\text{bias}} > V_{\text{depl}} + V_{\text{gl}} + V_{\text{offset,gl}}$). In that case, the increase of the electric field at every z is defined as:

$$E_{\text{offset}} = \frac{V_{\text{offset}}}{d_{\text{sensor}}} = \frac{V_{\text{bias}} - V_{\text{depl}} - V_{\text{gl}} - V_{\text{offset,gl}}}{d_{\text{sensor}}}. \tag{11}$$

Here d_{sensor} is the thickness of the entire sensor $d_{\text{sensor}} = d_{\text{bulk}} + d_{\text{imp}} + d_{\text{gap}}$. As mentioned, the gap is depleted first. The gap is assumed to have the same effective doping concentration as the bulk. Because $N_{\text{eff}} \propto \frac{V_{\text{depl}}}{d^2}$ (follows from Equation 8), the gap voltage is

$$V_{\text{gap}} = V_{\text{depl}} \frac{d_{\text{gap}}^2}{d_{\text{bulk}}^2}. \tag{12}$$

Once the gap is depleted, depletion of the p^+-implant starts. To deplete this, also the electric field in the gap is raised. This gives rise to the $V_{\text{offset,gap}}$. To calculate $V_{\text{offset,gap}}$ and V_{imp}, we use that they are areas in the shape of a rectangle and triangle respectively. Both have the same height h. Then, $V_{\text{offset,gap}} = h d_{\text{gap}}$ and $V_{\text{imp}} = \frac{1}{2} h d_{\text{imp}}$. We also know that $V_{\text{offset,gap}} + V_{\text{imp}} = V_{\text{gl}} - V_{\text{gap}}$. Thus, dividing $\frac{V_{\text{offset,gap}}}{V_{\text{imp}}}$ to get rid of h, we obtain equations for $V_{\text{offset,gap}}$ and V_{imp}. Then $V_{\text{offset,gap}}$ is given by

$$V_{\text{offset,gap}} = 2 V_{\text{imp}} \frac{d_{\text{gap}}}{d_{\text{imp}}}. \tag{13}$$

and V_{imp} is given by

$$V_{\text{imp}} = \frac{V_{\text{gl}} - V_{\text{gap}}}{1 + 2\frac{d_{\text{gap}}}{d_{\text{imp}}}}, \tag{14}$$

Once the gain layer is depleted, depletion of the bulk starts. Again, the electric field in the gain layer is also increased because of the depletion of the bulk. The formula for this voltage is derived similarly to Equation 13:

$$V_{\text{offset,gl}} = 2 V_{\text{depl}} \frac{d_{\text{gap}} + d_{\text{imp}}}{d_{\text{bulk}}}. \tag{15}$$

The voltage to deplete the gain layer is given as an input by the user.

Now that all voltages have been defined, the electric field can be calculated. To do this, z_{rel} is defined as the distance from the pn-junction, which is the start of the gap.

First, the electric field in the bulk is given by

$$E_{\text{bulk}}(z_{\text{rel}}) = -E_{\text{offset}} - \frac{2V_{\text{depl}}}{d_{\text{bulk}}^2}(d_{\text{bulk}} + d_{\text{gap}} + d_{\text{imp}} - z_{\text{rel}}), \tag{16}$$

where the last term follows from Equation 10. Moving on, the electric field in the implant is given by

$$E_{\text{imp}}(z_{\text{rel}}) = -E_{\text{offset}} - \frac{2V_{\text{depl}}}{d_{\text{bulk}}} - \frac{2V_{\text{imp}}}{d_{\text{imp}}^2}(d_{\text{gap}} + d_{\text{imp}} - z_{\text{rel}}). \tag{17}$$

Here, the second term is an additional offset because of $V_{\text{offset,gl}}$ with size $\frac{V_{\text{offset,gl}}}{d_{\text{gap}}+d_{\text{imp}}} = \frac{2V_{\text{depl}}}{d_{\text{bulk}}}$. Note that $E_{\text{bulk}}(d_{\text{gap}} + d_{\text{imp}}) = E_{\text{imp}}(d_{\text{gap}} + d_{\text{imp}})$ as expected.

Lastly, the electric field in the gap is given by

$$E_{\text{gap}}(z_{\text{rel}}) = -E_{\text{offset}} - \frac{2V_{\text{depl}}}{d_{\text{bulk}}} - \frac{2V_{\text{imp}}}{d_{\text{imp}}} - \frac{2V_{\text{depl}}}{d_{\text{bulk}}^2}(d_{\text{gap}} - z_{\text{rel}}). \tag{18}$$

Again, note that the third term is an additional offset of size $\frac{V_{\text{offset,gap}}}{d_{\text{gap}}} = \frac{2V_{\text{imp}}}{d_{\text{imp}}}$ and that as expected $E_{\text{imp}}(d_{\text{gap}}) = E_{\text{gap}}(d_{\text{gap}})$. Now the electric field has been defined in the entire sensor in the case of overdepletion.

4.1.2 Underdepletion of the bulk

In the case that the gain layer is depleted but the bulk is not, the sensor is not fully depleted. In this case, the equations in Section 4.1.1 do not hold. Specifically, the V_{offset} should be set to zero. Furthermore, the V_{depl} and $V_{\text{offset,gl}}$ should be adjusted accordingly. To do this, a new effective thickness of the bulk $d_{\text{eff,bulk}}$ as also drawn in Figure 13 is defined as

$$d_{\text{eff,bulk}} = \sqrt{\frac{V_{\text{bias}} - V_{\text{gl}}}{V_{\text{depl}}} + \left(\frac{d_{\text{gap}} + d_{\text{imp}}}{d_{\text{bulk}}}\right)^2}\, d_{\text{bulk}} - (d_{\text{gap}} + d_{\text{imp}}). \tag{19}$$

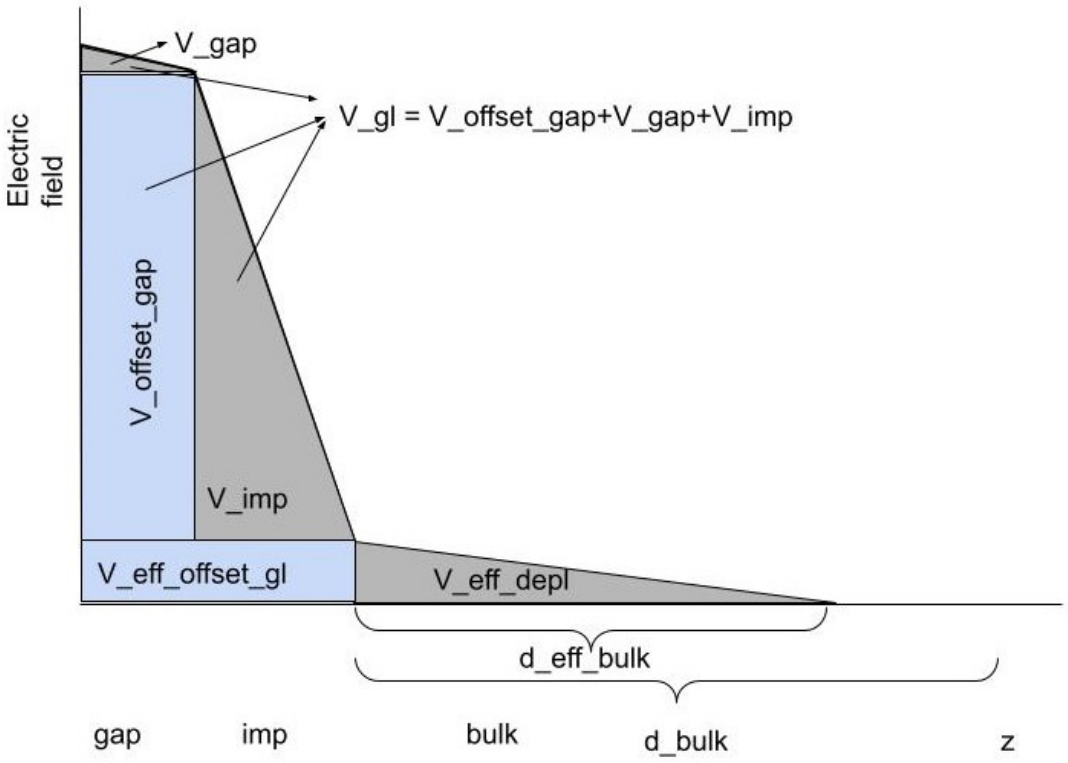

Figure 13: Definition of all the types of voltages in case of underdepletion of the bulk. Note that the coordinate system is shifted with respect to Figure 10. The z-axis is rotated and the absolute value of the electric field is considered.

This formula follows from the voltage left over after depleting the gain layer, which can be derived using that $\frac{V_{\text{eff,depl}}}{V_{\text{depl}}} = \frac{d^2_{\text{eff,bulk}}}{d^2_{\text{bulk}}}$ and the fact that $V_{\text{eff,offset,gl}}$ is a rectangle with width $d_{\text{gap}} + d_{\text{imp}}$

and height $\frac{2V_{\text{depl}}}{d_{\text{bulk}}}\frac{d_{\text{eff,bulk}}}{d_{\text{bulk}}}$ to be

$$V_{\text{bias}} - V_{\text{gl}} = V_{\text{eff,depl}} + V_{\text{eff,offset,gl}} = \frac{V_{\text{depl}}}{d_{\text{bulk}}^2}\left(d_{\text{eff,bulk}}^2 + 2(d_{\text{gap}} + d_{\text{imp}})d_{\text{eff,bulk}}\right). \tag{20}$$

Here, $V_{\text{eff,depl}}$ and $V_{\text{eff,offset,gl}}$ are the effective voltage boxes in the case of underdepletion. This is a quadratic equation in $d_{\text{eff,bulk}}$ can be solved for $d_{\text{eff,bulk}}$ to obtain Equation 19.
Now also the V_{depl} can be adjusted to

$$V_{\text{eff,depl}} = \frac{V_{\text{bias}} - V_{\text{gl}}}{1 + 2\frac{d_{\text{gap}}+d_{\text{imp}}}{d_{\text{eff,bulk}}}} \tag{21}$$

and, similar to the calculation of Equation 15, $V_{\text{offset,gl}}$ becomes

$$V_{\text{eff,offset,gl}} = 2V_{\text{eff,depl}}\frac{d_{\text{gap}} + d_{\text{imp}}}{d_{\text{eff,bulk}}}. \tag{22}$$

Now, equations 16, 17 and 18 can be used with these effective values to calculate the field within the effective region of the sensor ($d_{\text{gap}} + d_{\text{imp}} + d_{\text{eff,bulk}}$). Outside this region, the field is zero.

4.1.3 Underdepletion of the gain layer

In the case that the bias voltage is low, it is possible that the gain layer is not fully depleted. In this case, the same technique in 4.1.2 can be used to calculate effective values by considering the effective thickness of the gap $d_{\text{eff,gap}}$.
In the case that the gap is not even depleted, the bias voltage only partly depletes the gap and nothing else, thus all voltages are set to zero except for

$$V_{\text{bias}} = V_{\text{eff,gap}} = V_{\text{eff,gl}}, \tag{23}$$

and the effective gap thickness follows from $|N_{\text{eff}}| \propto \frac{V_{\text{eff,gap}}}{d_{\text{eff,gap}}^2} = \frac{V_{\text{gap}}}{d_{\text{gap}}^2}$ and Equation 23:

$$d_{\text{eff,gap}} = \sqrt{\frac{V_{\text{bias}}}{V_{\text{gap}}}}d_{\text{gap}}. \tag{24}$$

The case that the gap is depleted, but the implant is not is drawn in Figure 14. Then, the effective implant thickness becomes

$$d_{\text{eff,imp}} = \sqrt{\frac{V_{\text{bias}} - V_{\text{gap}}}{V_{\text{imp}}} + \left(\frac{d_{\text{gap}}}{d_{\text{imp}}}\right)^2}d_{\text{imp}} - d_{\text{gap}}. \tag{25}$$

This follows from a similar reasoning as Equation 19 was obtained. Furthermore, all voltages are set to zero except for $V_{\text{eff,gl}} = V_{\text{bias}}$ and the implant voltage becomes

$$V_{\text{eff,imp}} = \frac{V_{\text{bias}} - V_{\text{gap}}}{1 + 2\frac{d_{\text{gap}}}{d_{\text{eff,imp}}}} \tag{26}$$

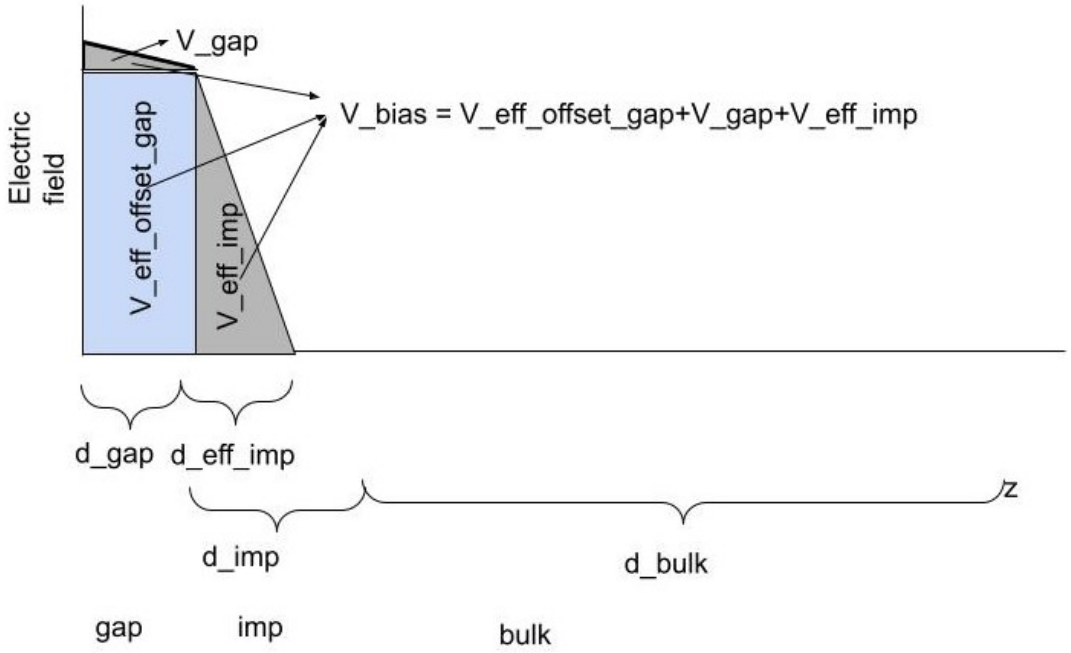

Figure 14: Definition of all the types of voltages in case of underdepletion of the gain layer when the gap is depleted. Note that the coordinate system is shifted with respect to Figure 10. The z-axis is rotated and the absolute value of the electric field is considered.

Again, these effective values can be used in equations 16, 17 and 18 to obtain the equations for the electric field for $z < d_{\text{eff,gap}} + d_{\text{eff,imp}}$ in case of underdepletion. Outside of effective thickness $d_{\text{eff,gap}} + d_{\text{eff,imp}}$, the field is zero.

4.2 Gain reduction and electric field screening implementations

As mentioned at the start of this section, two different functions have been added to the Allpix Squared framework. They simulate the screening of gain in the gain layer. They are called GainReduction and ElectricFieldScreening. Each function currently only contains one model. They are called by the propagation module as seen in Figure 15. Both perform the same task. In Section 7, the two functions are analyzed and compared. Both functions implement the parametrization in [2], but each in a different way. They both require the density of eh-pairs deposited in the gain layer, n_{eh}, and a prediction of the gain obtained by electrons in the gain layer, the predicted gain G_{pred}. The predicted gain acts as the average gain in Equation 5. Before propagation, the predicted gain is calculated from the electric field in the gain layer and the density of eh-pairs is calculated from the deposited charge message. These two values can then be used in Equation 5 or in Equation 4. For GainReduction, Equation 5 is used. For ElectricFieldScreening, Equation 4 is used. Their workings should be fairly similar, because Equation 5 follows from Equation 4 by using the Chynoweth parametrization with Overstraeten deMan coefficients for the impact ionization.

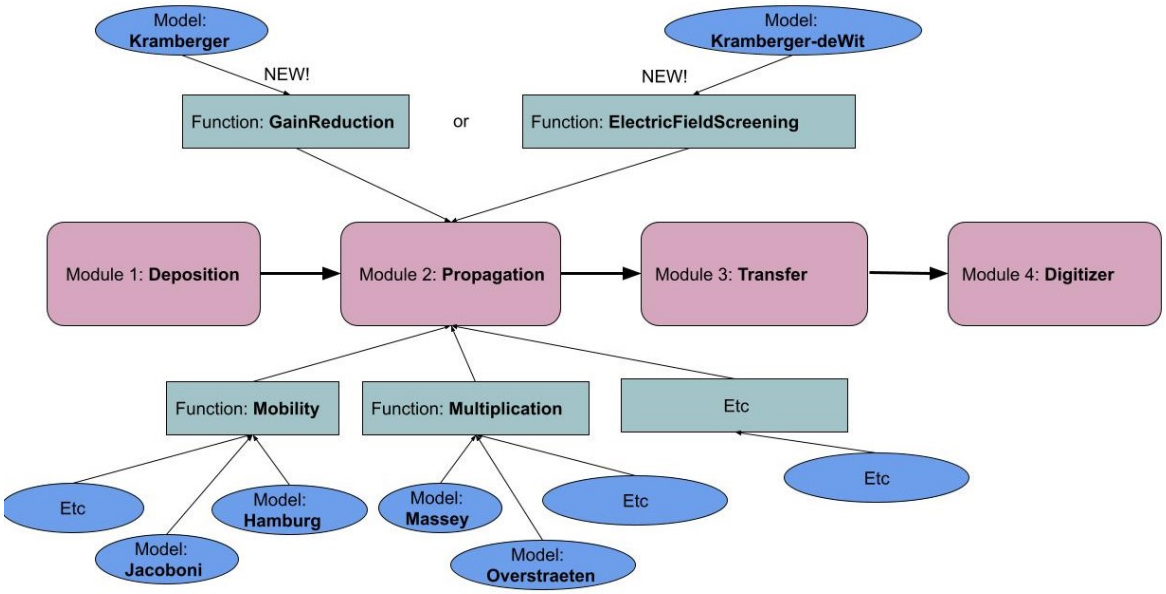

Figure 15: Part of an generic simulation with GainReduction and ElectricFieldScreening. The functions GainReduction and ElectricFieldScreening are incorporated in the structure in the same way that the functions such as Mobility and Multiplication are included.

The first function, GainReduction, acts upon the gain G of every charge group and reduces this by a factor to G_{red}. The reduction factor r is then defined by $G_{\text{red}} = G^{1-bn_{\text{eh}}} = G \cdot r(G)$.

The second function, ElectricFieldScreening, calculates a constant perturbation of the electric field ΔE from Equation 4 before propagation of the charge groups starts. For every charge group and for every step in the gain layer, the local gain is calculated from the perturbed electric field $E - \Delta E$.

4.2.1 Detailed workings of GainReduction and ElectricFieldScreening

GainReduction takes the following input parameters:

- gain_reduction_model. For now there is only one choice, namely the Kramberger model. This is also the default.
- gain_reduction_threshold. This is the minimal density of charge in order to consider gain reduction. Defaults to infinity.
- gain_reduction_beam_shape. The options are "gaussian", "minmax" (for a round flat beam) or "square". Defaults to "gaussian".
- thickness_gain_layer. For now the function requires a user input of the approximate thickness of the gain layer which the function uses. Defaults to 0.
- gain_reduction_steps. The amount of steps taken through the gain layer to calculate the predicted gain. Defaults to 100.

- gain_reduction_adjusted_bvalue. The choice between the hole and electron E_C value used for the calculation of parameter b of Equation 5. "true" means using the electron value $123\,\mathrm{V\,\mu m^{-1}}$, "false" means using the hole value $203\,\mathrm{V\,\mu m^{-1}}$. Defaults to "true".

ElectricFieldScreening takes roughly the same input parameters:

- electric_field_screening_model. For now there is only one choice, namely the Kramberger-deWit model. This is also the default.
- electric_field_screening_threshold. This is the minimal density of charge in order to consider electric field screening. Defaults to infinity.
- electric_field_screening_shape. The options are "gaussian", "minmax" (for a round flat beam) or "square". Defaults to "gaussian".
- thickness_gain_layer. For now the function requires a user input of the approximate thickness of the gain layer which the function uses. Defaults to 0.
- electric_field_screening_steps. The amount of steps taken through the gain layer to calculate the predicted gain. Defaults to 100.

Both functions currently contain only one model. However, it is very easy to add a new model. In order to calculate the perturbation of the electric field ΔE or the reduction r, it is necessary to know the density of eh-pairs of the deposition in the gain layer. We also need an estimate of the gain to know the total amount of secondary charges that screen the electric field.

Before the propagation modules starts to propagate all charges one by one, it first calculates the density of charges in the gain layer at the moment of deposition. This is calculated from the deposited charge message. The deposition time of charges is ignored, the charges are assumed to be deposited all at the same time. The implementation mainly works with the surface density, calculated as

$$n_{2D} = \frac{Q_{eh}}{A}, \tag{27}$$

where A is the surface area covered by the charges and Q_{eh} is the amount of electron-hole pairs in the gain layer. The charges in the gain layer are counted to obtain total charge Q_{gl} and their x and y coordinates are stored. Because Q_{gl} contains both the electrons and the holes, $Q_{eh} = \frac{Q_{gl}}{2}$. There are three ways the function can calculate the area. If the user specifies "minmax", then the maximum and minimum x and y coordinate of all charges in the gain layer are found and the area is calculated as

$$A = \frac{\pi}{4}(max_x - min_x)(max_y - min_y). \tag{28}$$

If the user specifies "square", the minimum and maximum values are again found and the area is calculated as

$$A = (max_x - min_x)(max_y - min_y). \tag{29}$$

If the user specifies "gaussian", the standard deviation σ is calculated from the x and y coordinate vectors. Then, $FWHM = 2.355\sigma$ in both x and y directions for gaussian beams and

$$A = \pi(\frac{FWHM_x FWHM_y}{4}). \tag{30}$$

One can simply take $n_{3D} = \frac{n_{2D}}{d_{gl}}$ to obtain the volumetric density.

The predicted gain is calculated from the start of the gain layer. N (default 100) steps are taken through the gain layer with E_i the electric field value at that step. Then, the accumulated gain is calculated as

$$G_\mathrm{pred} = \prod_{i=1}^{N} G_\mathrm{local}(E_\mathrm{i}, T, \Delta l), \qquad \Delta l = \frac{d_\mathrm{gl}}{N}. \tag{31}$$

The impact ionization model is chosen by the user. The average electric field E_ave is also calculated in this process using $E_\mathrm{ave} = \frac{1}{N}\sum_{i=1}^{N} E_\mathrm{i}$. This average electric field is used in the GainReduction function as the constant field that is assumed in Equation 5.

The surface density of secondary eh-pairs in the gain layer is approximately $(G_\mathrm{pred} - 1)n_\mathrm{eh,2D}$. Using Equation 4 with $n_\mathrm{eh,2D} = d_\mathrm{gl} n_\mathrm{eh}$, the perturbation of the electric field is

$$\Delta E = \frac{e_0}{\epsilon\epsilon_0}(G_\mathrm{pred} - 1)n_\mathrm{eh,2D}. \tag{32}$$

The reduction is

$$r(G) = G^{-bn_\mathrm{eh,2D}} \qquad b = \frac{E_\mathrm{C}}{E_\mathrm{ave}^2}\frac{e_0(G_\mathrm{pred} - 1)}{\epsilon\epsilon_0}. \tag{33}$$

4.2.2 Assumptions and comparison

As the implementation is based on the approximation in [2], the assumptions made in this implementation on the physical processes are the same as those in [2]. Below is a list of the basic assumptions used for both the GainReduction and the ElectricFieldScreening functions. Both functions assume:

- an n-on-p LGAD, thus electrons moving towards the gain layer.
- a parallel plate capacitor approximation for the secondary charge carriers in the gain layer as described in Section 2.3.1.
- a one dimensional electric field in the z-direction with the internal field in the $-z$-direction.
- a definable gain layer of fixed thickness.
- that the multiplication of holes does not contribute to the gain reduction (predicted gain is based on gain of electrons alone).
- that the gain layer is always at the top of the sensor.
- all charges are deposited at the same time.
- there is no time dependence. Only in the sense that the density is calculated from the charges in the gain layer before propagation. Thus injection of charges in the backplane (like TCT red back injection) results in no gain reduction.
- the calculation of the density only works for gaussian beam shapes perpendicular to the detector or for oval/square flat beams with the principal axes in the x and y direction.

Aside from these, the GainReduction function makes use of more assumptions which the ElectricFieldScreening function does not. This is an advantage of the ElectricFieldScreening function. The main differences are:

- GainReduction also assumes a constant electric field in the gain layer, namely $E = \frac{V_{\text{gl}}}{d_{\text{gl}}} \approx E_{\text{ave}}$. ElectricFieldScreening uses the field provided by the user.
- GainReduction is based on a first order Taylor approximation for $\Delta E << E$. ElectricFieldScreening does not.
- GainReduction uses the Chynoweth model for the impact ionization coefficient with the parameters of Overstraeten deMan. ElectricFieldScreening uses the model for impact ionization chosen by the user.

5 Setup

An overview of the workings of the new implementations has been given. In order to test them, multiple simulations are performed. To test the new electric field type, it has been compared to TCAD simulations of the HPK2-W25. To test the gain reduction implementations, the experiments performed in [2] are simulated and we perform our own measurements of the HPK2-W36 which we simulate as well. In this section, a general description of the geometry used in all simulations is given. Also, more details on the setups of both the electric field simulations and the gain reduction simulations are given.

5.1 The geometry

In this thesis, unless otherwise specified, a single monolithic pad detector is used. It has a thickness of 50 µm and a pixel size of 800x800 µm^2. There is no excess material. Because of the large pixel size, it is valid to assume a one dimensional electric field within this sensor. This detector type is stored in the file `LGADdiode.conf`. No details on the doping are needed because the electric field is configured separately. For all simulations, this detector is placed in the center of the world frame and the laser is placed at $z = 200$ mm, pointing in the $-z$-direction, passing through the detector perpendicularly. Unless otherwise specified, infrared light is used with a wavelength of 1064 nm. The pulse duration is 350 ps. The deposition of such an infrared laser is shown in Figure 16.

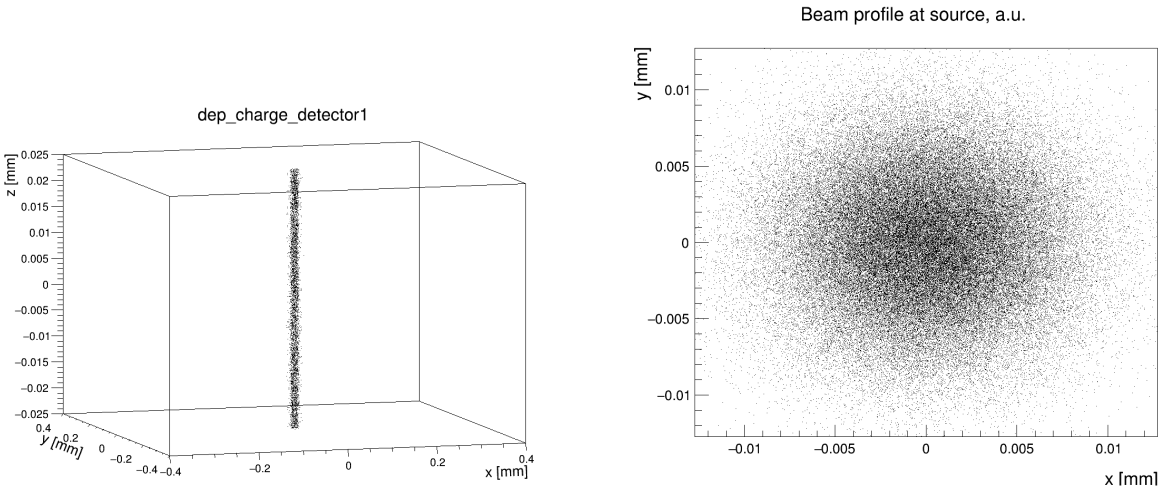

(a) Volume (b) Cross section at the source

Figure 16: Deposited charges for an infrared laser with $1 \cdot 10^5$ photons.

5.2 Setup of the electric field simulations

To verify the validity of the implementation of the gain layer electric field type, a simulation of the HPK2-W25 LGAD has been done. This LGAD has a thickness of 50 µm and gain layer of approximately 2 µm. The gain layer depletion voltage is 54 V and the bulk depletes in 7.2 V [22]. The electric field is calculated for different bias voltages and is compared to TCAD simulations.

5.3 Setup of the gain reduction simulations

In Section 6 and 7, simulations are performed on the HPK-T3.1 and HPK-T3.2. They are both LGADs with a thickness of 50 µm. The HPK-T3.1 has a gain layer depletion voltage of 41 V and the bulk is depleted in approximately 5 V. In [2], the gain layer thickness is estimated to be 1.5 µm. The HPK-T3.2 has a gain layer depletion voltage of 55.5 V and the bulk is also depleted in approximately 5 V [2]. In [2], the gain layer thickness is estimated to be 2 µm. For simulations, the new electric field type gain layer is used to set the electric field in the ElectricFieldReader module. The depletion voltages above are used and the thickness of the gap and thickness of the implant are tweaked such that the thickness of the gain layer ($d_{\text{gl}} = d_{\text{gap}} + d_{\text{imp}}$) is in agreement with the estimations in [2] and such that unreduced gain in the accumulated gain algorithm matches literature.

For simulations done in the accumulated gain algorithm, a pulse of $8 \cdot 10^4$ photons from the infrared laser is simulated using the DepositionLaser module. For an infrared laser and a thin detector, only a small fraction of these photons create charge carriers in the silicon. The propagation is done using the TransientPropagation module and diffusion is turned off. In the probability based algorithm, the laser shoots $4 \cdot 10^5$ photons. The propagation is performed by the GenericPropagation module and diffusion is turned on. GenericPropagation is a faster module so the amount of photons could be increased which is needed for a statistical algorithm like the probability based algorithm. In a simulation, one instance of the deposition module is run and from the output message of this module, multiple instances of the propagation module are ran. The different instances have different settings which allows us to see the propagation for both functions using the same deposition.

The time step is set to 0.1 ps in order to have an enough steps through the very small gain layer. The laser power is kept constant and the density is varied by changing the configuration of the beam waist in the DepositionLaser module.

Unless otherwise specified, the gain of a simulation is taken to be the mean of the gain distribution of the primary electrons. This means that it is assumed that the holes do not multiply. This assumption is in line with the assumptions made in [2]. For computational reasons, also the production of the secondary charge carriers is turned off. This affects the total charge but it does not affect the gain of the primary electrons and reduces the computation time and power by a very significant factor.

5.4 Setup of the simulations of our own measurements

The simulation uses GenericPropagation with the probability based algorithm with diffusion and the creation of secondary charges is also turned on. The gain is now calculated as the amount of charges after propagation divided by the amount of charges present at deposition. The Massey_optimized model is used since this model was developed for these detectors. According to the TCAD input, the thickness of the gain layer is approximately 2.2 µm. This value is used in the GainReduction

and ElectricFieldScreening function. Because the secondary charges are propagated which takes extra time, the number of photons is reduced to $2 \cdot 10^5$.

6 Results

In this section, the results of the new electric field type are presented. After that, a brief summary of the results from the simulations of the HPK-T3.1 and the HPK-T3.2 is given. These results are investigated in more depth in Section 7.

6.1 Results of the electric field implementation

A TCAD simulation of the HPK2-W25 LGAD was done in [22]. Figure 17 shows the results. From this, the p^+-implant is estimated to be 0.5 µm and the gap thickness is estimated to be 1.5 µm. For various bias voltages the results of the gain layer electric field implementation (formalism described in Section 4.1) in Allpix Squared can be seen in Figure 18. It should be noted that the results in Figure 17 are the absolute value of the electric field and that the gain layer is assumed to be on the left side of the figure, whereas it is at the right side of the figure in the Allpix Squared simulation. It is clear that the order of magnitude and the behavior of the approximation are correct. The gain layer is depleted at the same voltage as for the TCAD simulation and both obtain an electric field of around 300 kV cm^{-1} after depletion. Slight differences in absolute value are because the size of the gap and p^+-implant are a rough estimate. Of course, also the shape of the approximation is less smooth than that of the TCAD simulation, because of the doping boxes assumption for this approximation.

The implementation of the gain layer electric field is an approximation and should also be treated this way. In real LGADs, the effective doing in the p^+ implant is not uniform. Because the gain layer is very thin, it is also very sensitive to slight changes in the thickness of the gap d_{gap} or p^+-implant d_{imp}. Thus, these values need to be known or tweaked to obtain the expected gain.

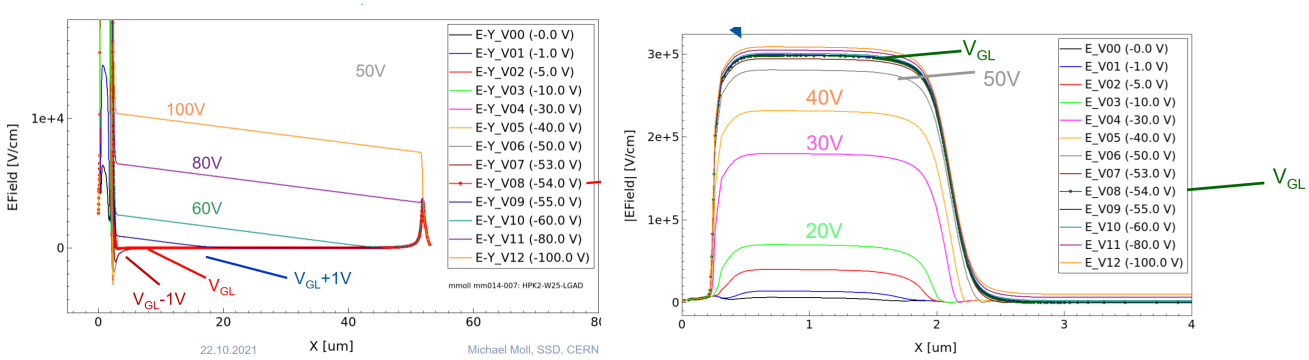

(a) Bulk (b) Gain layer

Figure 17: A TCAD simulation for the electric field of HPK2-W25 at various bias voltages. The absolute value of the electric field is depicted [22].

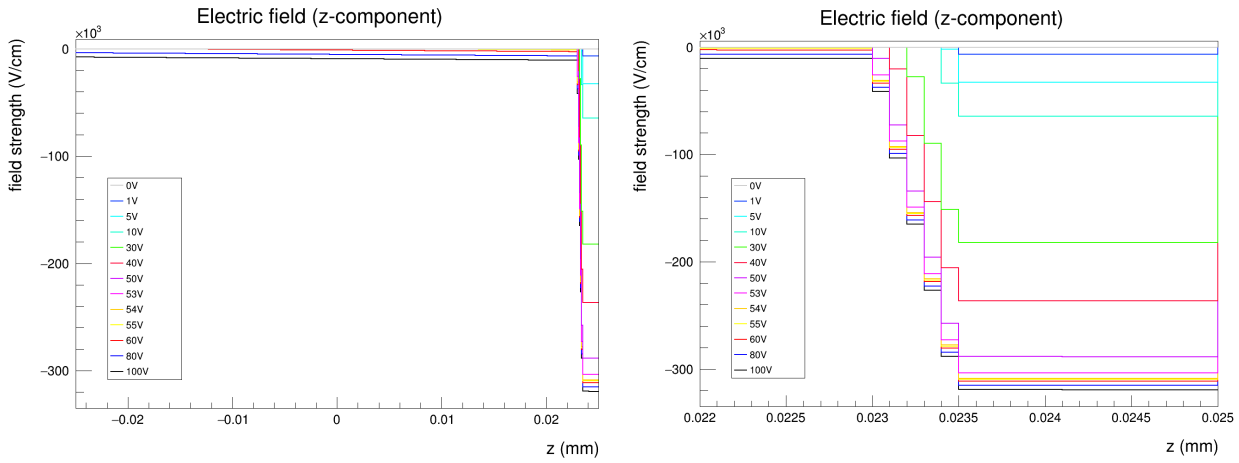

(a) Bulk

(b) Gain layer

Figure 18: Electric field of a 50 µm LGAD with a gap of 1.5 µm and an implant of 0.5 µm with bulk depletion voltage 7.2 V and gain layer depletion voltage of 54 V as to reproduce the HPK-W25.

6.2 Results of the gain reduction implementation

Many simulations have been performed on the HPK-T3.1 and the HPK-T3.2. The simulations have been done for both algorithms and both functions but also for various bias voltages and impact ionization models. The results of a subset of these simulations is put forth in this section. The plots show the gain as a function of the volumetric charge carrier density in the gain layer as calculated by the functions. The results of all simulations can be found in Appendix C. Figure 19 shows the results of a simulation of the HPK-T3.1 in the old accumulated gain algorithm at a bias voltage of 80 V using the Overstraeten model for impact ionization. Both GainReduction and ElectricFieldScreening are shown. The results from [2] are also displayed. Figure 20 shows the same setup in the new probability based algorithm.

From these plots we can conclude that the GainReduction function matches the results from [2] very well in both algorithms. The ElectricFieldScreening function underestimates the reduction of the gain. As expected, in case neither the GainReduction nor the ElectricFieldScreening function is turned on, there is no dependence of the gain on the density. An in depth analysis of these results is given in the next section.

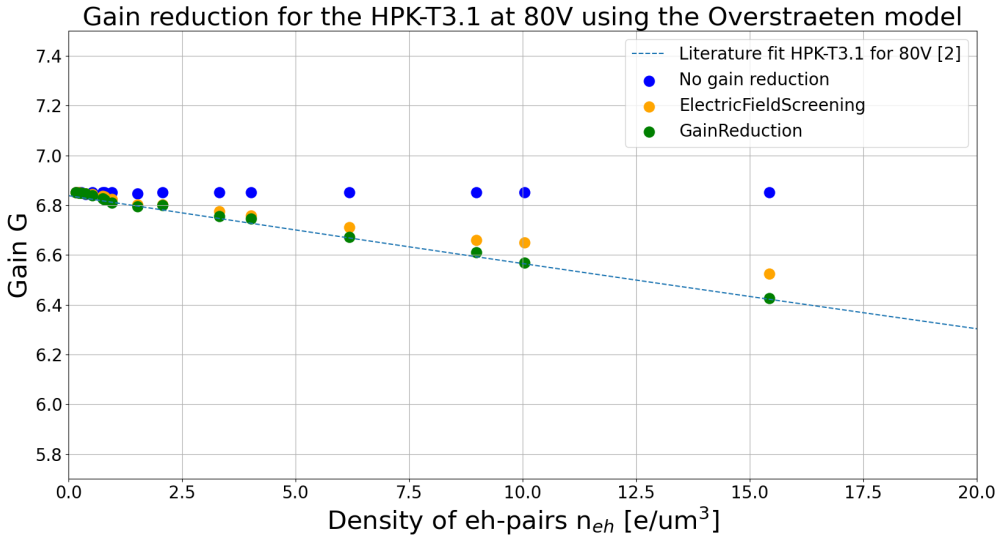

Figure 19: Simulation in the accumulated gain algorithm of the HPK-T3.1 at 80 V using the Overstraeten model for impact ionization and d_{imp} =0.41 µm and d_{gap} = 1.09 µm. The simulation is performed for both the GainReduction and the ElectricFieldScreening function. The plot also shows the results from [2] and the gain in case no gain reduction is simulated.

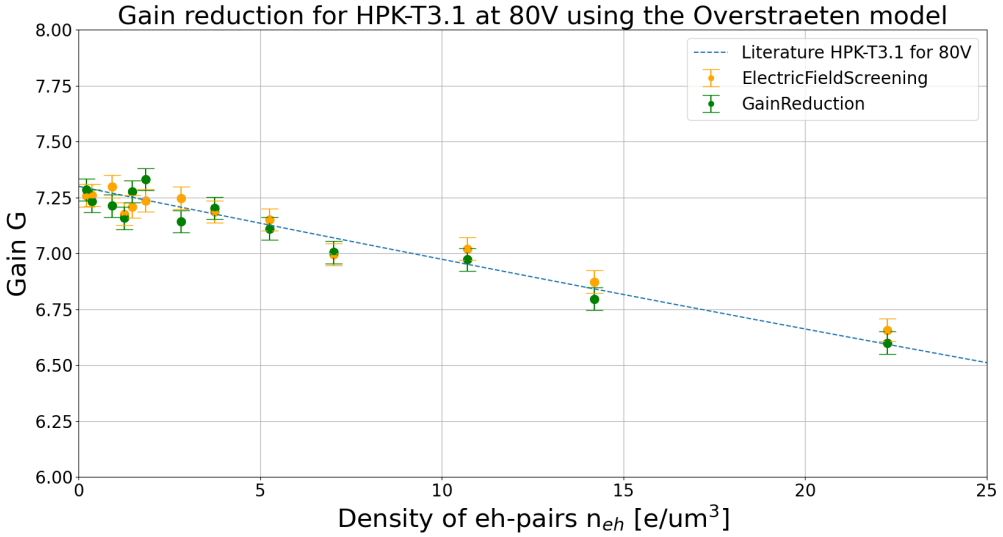

Figure 20: Simulation in the probability based algorithm of the HPK-T3.1 at 80 V using the Overstraeten model for impact ionization. The same configuration is used as for the accumulated gain algorithm. The simulation is performed for both the GainReduction and the ElectricFieldScreening function. The results from [2] corrected for the slightly higher unreduced gain for the probability based algorithm are shown.

7 Analysis of the gain reduction simulations

This section aims to discuss in depth the findings in Section 6.2. This is done by also considering the HPK-T3.2 LGAD and repeating similar simulations with different settings. First the calculations of the density and predicted gain are discussed.

7.1 Density calculation

In case there are few charge carriers in the gain layer, the calculation of the $FWHM$ and thus the eh-pair density might be inaccurate. The convergence has been investigated. In order to do so, front side red injection from the DepositionLaser module is used. The beam waist and thickness of the gain layer is kept fixed and the amount of photons is increased, thus increasing the amount of created charge groups. This increases the density in the gain layer whilst maintaining a gaussian distribution. The surface density calculated by the functions is compared to the theoretical surface density that would be expected from the configuration in the DepositionLaser module. The theoretical density can be calculated from the beam waist value and the amount of charge that the DepositionLaser module deposits. The ratio of these two densities should converge to 1 as the amount of charge groups increases. The result can be seen in Figure 21. It has been done for two different configurations for the beam waist in the DepositionLaser module. As expected, the ratio indeed converges to 1. This happens after around $2 \cdot 10^4$ deposited charge groups in the gain layer. The input beam waist does not play a significant role in the convergence. In the simulations done in this work, the amount of deposited charge groups in the gain layer is much lower than $2 \cdot 10^4$. This choice was made to reduce the computation time of the simulation. This does not impact the results since the true density (calculated by the functions) was used in the final plots.

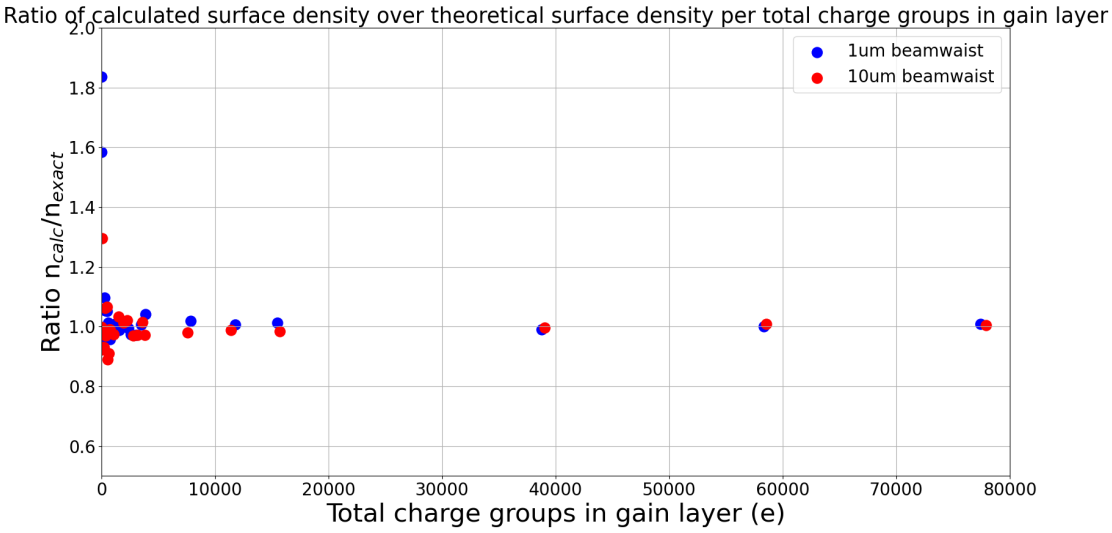

Figure 21: Ratio of the surface density in the gain layer calculated by GainReduction and ElectricFieldScreening and the theoretical surface density from the DepositionLaser configuration.

7.2 Predicted gain calculation

As mentioned, the gain is predicted by taking N (default 100) steps through the gain layer and calculating the accumulated gain of an electron. This method includes the multiplication of secondary electrons, but not the multiplication of secondary holes, which is a reasonable approximation for low gain. For various settings, the different gains are compared in Table 1. G_0 refers to the unreduced gain calculated by the functions. G_{pred} is used in the program in the way that $\bar{G}$ is used in [2], thus it is desirable for G_0 and G_{pred} to be fairly similar. However, they do not have the same physical meaning. The meaning of $\bar{G}$ is explained in Section 2.3.1 and G_{pred} is the gain obtained from only the gain layer. Both however, should be slightly smaller than G_0.

Because the predicted gain is calculated similarly to the workings of the accumulated gain algorithm and because the ratio of d_{gap} and d_{imp} of the electric field setup have been adjusted to obtain the correct G_0, these values agree fairly well. The G_{pred} slightly underestimates the G_0, but this could be explained by the fact that it does not take into account any multiplication in the bulk. G_{pred} is not exactly $\bar{G}$, because, as mentioned, they do not have the same physical meaning. Especially for higher gain, $\bar{G}$ is lower than G_{pred}.

The unreduced gain values G_0 for the probability based algorithm do not agree as well as for the accumulated gain algorithm. There could be several explanations for this. First of all, the electric field layout has been tweaked to match the unreduced gain of the accumulated gain algorithm with the measurements of [2]. For simulations in the probability based algorithm, the same electric field is used. However, it was observed that the unreduced gain in both algorithms are not equal. The reason for this is not fully understood and further elaborated on in Section 7.4. Secondly, the gain is now taken to be the average of an exponential fit over the gain of the primary electrons, because the charge groups no longer all have the same accumulated gain.

Device	II model	V_{bias}	G_0 AGA	G_0 PBA	G_0 [2].	G_{pred}	$\bar{G}$ [2]
HPK-T3.1	Massey	80 V	6.805	7.45	6.838	6.686	6.8
HPK-T3.1	Overstraeten	80 V	6.851	7.3	6.838	6.731	6.8
HPK-T3.1	Massey	70 V	6.564	7.1	6.612	6.447	6.5
HPK-T3.1	Overstraeten	70 V	6.549	6.95	6.612	6.435	6.5
HPK-T3.2	Massey_optimized	80 V	33.21	37.5	33	32.286	31.3
HPK-T3.2	Massey_optimized	90 V	40.14	45.0	40.08	38.965	37.7

Table 1: Gain comparisons for accumulated gain algorithm. II model means impact ionization model. G_0 is the unreduced gain. AGA stands for the accumulated gain algorithm. PBA stands for the probability based algorithm. $\bar{G}$ [2] is the average gain value measured in [2].

7.3 ElectricFieldScreening versus GainReduction

In all simulations done in for this work, it is observed that the ElectricFieldScreening function underestimates the gain reduction compared to the GainReduction function. This is because of the electric field profile. For the GainReduction function, an average electric field is assumed over the gain layer. Effectively, the GainReduction function reduces this constant electric field by a perturbation ΔE and calculates the reduction factor from this reduced field. The ElectricFieldScreening function reduces the actual electric field in the gain layer by a constant perturbation ΔE. The

gain of a step in field E goes as $G \sim e^{e^{-1/E}}$. The shape of this function is drawn in Figure 22. Calculating the gain from a non-constant electric field is not the same as calculating it from the average value of that non-constant electric field.

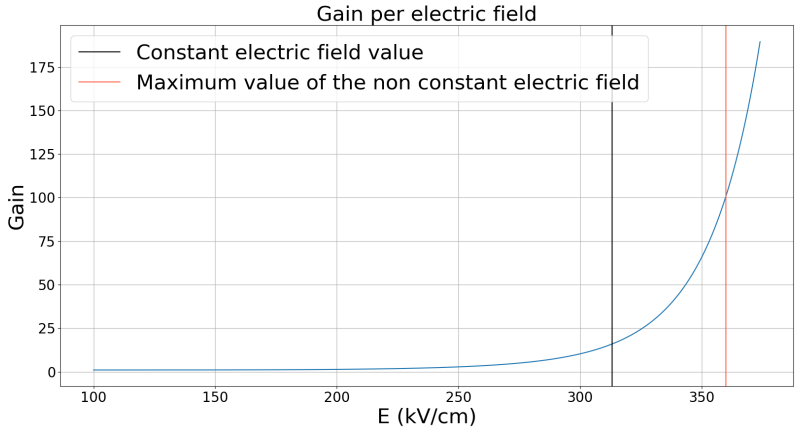

Figure 22: Gain G as a function of electric field using the Overstraeten model for impact ionization for a step of 2 µm through a constant electric field E.

This is verified by considering two types of electric field in the gain layer, displayed in Figure 23. The gain layer starts where the electrons enter the gain layer. This is set to $z = 0$. The gain layer ends at the pn-junction at $z = 2$. We consider a constant electric field and a non-constant field consisting of one linear part and one constant part. The constant electric field mimics the average field assumed by the GainReduction function. The non-constant electric field better approximates an actual gain layer electric field with the p^+-implant between $z = 0$ and $z = 1$ and a gap between $z = 1$ and $z = 2$. Both are decreased by the same variable ΔE, as also shown in Figure 23 by the dashed lines. The gain of the fields is calculated by taking smalls steps Δl from the beginning to the end (in this case from 0 to 2) and accumulating the gain similar to the accumulated gain algorithm using the Overstraeten deMan parametrization. The formula for the local gain used to obtain the final accumulated gain is the following equation.

$$G = e^{\alpha(E-\Delta E)\Delta l} \qquad \alpha = a_0 e^{-\frac{E_C}{E-\Delta E}}. \tag{34}$$

The constant electric field was chosen such that the gain at $\Delta E = 0$ of this electric field was the same as that of the non-constant electric field. The final accumulated gain as a function of the perturbation of the electric field ΔE has been plotted in Figure 24a (where $\Delta E \propto n_{\text{eh}}$ because of Equation 4). It confirms that the reduction of gain is dependent on the electric field shape. The non-constant electric field, which is an approximation of the electric field shape of a gain layer with a gap, results in less gain reduction.

To see why exactly the non-constant electric field always results in less reduction than a constant electric field, we need to look at the accumulated gain whilst stepping through the gain layer, and not only the final accumulated gain. Every step, we calculate the reduction factor. Similar to the accumulated gain, we can also accumulate this reduction factor. This is plotted in Figure 24b for both electric field shapes. It shows that the reason that the reduction is less for the non-constant electric field is because there is almost no reduction in the p^+-implant (between $z = 0$

and $z = 1$). This is again because the gain as a function of the electric field is non-linear and there is very little gain for low electric field. This cannot be compensated anymore in the gap. That is why the ElectricFieldScreening function, working on a non-constant electric field, underestimates the reduction compared to the GainReduction function.

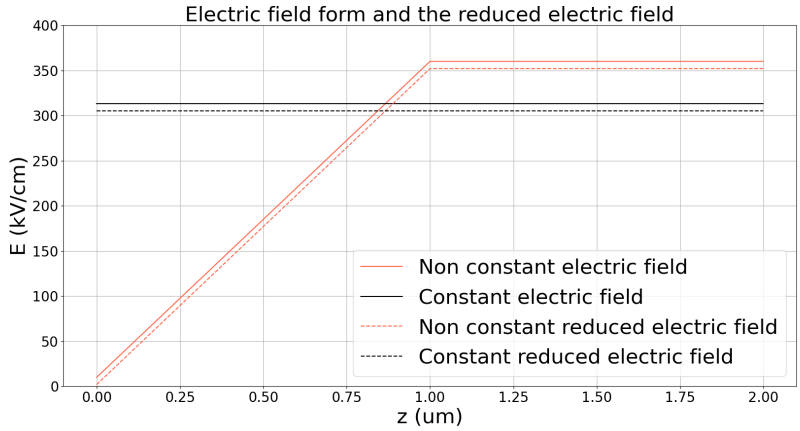

Figure 23: Electric field shape

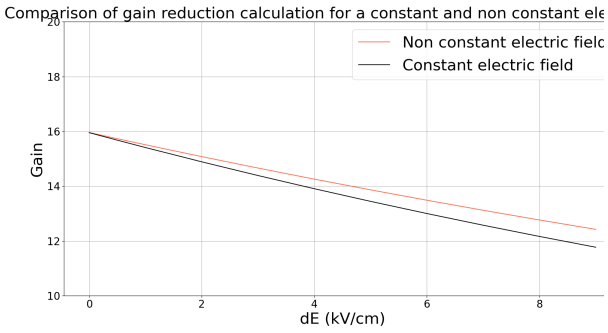

(a) Gain reduction as a function of ΔE

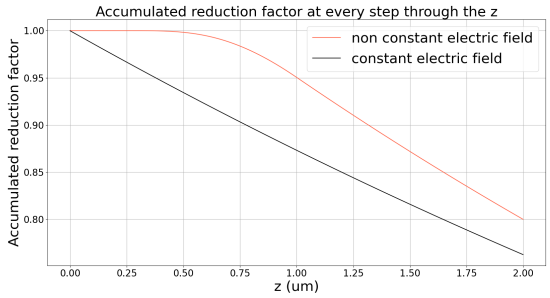

(b) Accumulated reduction factor. It is accumulated from $z = 0$ to $z = 2$.

Figure 24: On the left: gain as a function of the perturbation of the electric field ΔE. On the right: the accumulated reduction factor as we step through the gain layer.

7.4 Accumulated gain algorithm versus probability based algorithm

As explained in Section 3.2, the reason a newer version of the gain algorithm, the probability based algorithm, was created was because there were inconsistencies in the accumulated gain algorithm. There are two main issues with the accumulated gain algorithm. Firstly, it is non-statistical whereas impact ionization is a statistical process. Secondly, secondary charges were only produced when the accumulated gain crosses an integer value. While the gain of a charge carrier group is calculated using floating point precision, the number of secondaries produced is the floored integer of the gain. This raises a problem when considering gain reduction. For example, if the gain would be reduced from 2.3 to 2.1, there would be no difference in the amount of secondaries created. If it were reduced from 2.1 to 1.9, then there would be a large difference, as the gain no longer crosses the integer

threshold 2 and as a result no new charge carriers are created. Therefore, we cannot look at the induced charge as a result of produced secondaries when simulating gain reduction. Instead, the gain considered in this thesis is the mean of the gain distribution of the primary electrons, which is not affected by this problem with rounding down. These two issues of statistics and rounding are resolved in the new probability based algorithm.

Because of the statistics, the data of the probability based algorithm is less stable than that of the accumulated gain algorithm. Reducing these fluctuations by depositing more charges was not possible because of computation time reasons. However the general trend of reduction is still clearly visible and conclusions can still be drawn from the results of these simulations.

A reoccurring issue throughout this work is the discrepancy between the unreduced gain of the accumulated gain algorithm and that of the probability based algorithm (see Figure 19 and 20). The simulations done for this thesis are done for both algorithms, but the gain at small charge carrier density, the unreduced gain, does not match. This inconsistency is not fully understood. It raises a problem when investigating gain reduction, because the gain reduction is determined by the predicted gain, which is always calculated as an accumulated gain. For small gain, this difference is also small and so also the effect on the gain reduction is absorbed into the statistical uncertainty. For large gain, however, the discrepancy is also larger and thus also the effect on the gain reduction. This is observed in the simulations of the HPK-T3.2, which has a gain around 33 in the accumulated gain algorithm and measurements and a gain of 37 in the probability based algorithm. The results of simulations of the HPK-T3.2 in both algorithms are displayed in Figure 25. The literature function in Figure 25a is from [2] and the literature function in 25b is also from [2], but is corrected for the dissimilar unreduced gain of the probability based algorithm. In the accumulated gain algorithm, the predicted gain matches the unreduced gain. Thus, the gain reduction is accurately simulated by the GainReduction function. Since the probability based algorithm overestimates the gain compared to the predicted gain (33), the gain reduction is underestimated as $b(G_{\text{pred}})$ is too small.

However, in the probability based algorithm, the predicted gain is still approximately 33, but the unreduced gain is now 37. Thus, the gain reduction is underestimated because $b(G_{\text{pred}})$ is now too small.

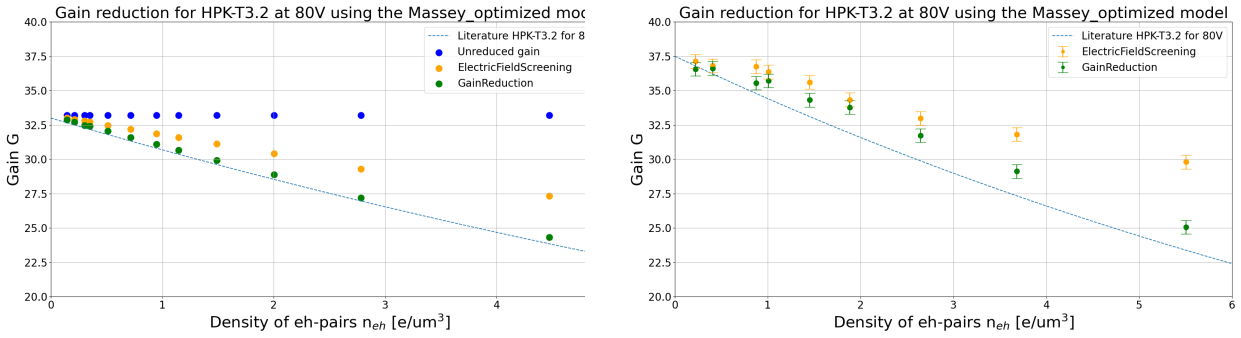

(a) Accumulated gain algorithm

(b) Probability based algorithm

Figure 25: Simulation of the HPK-T3.2 at a bias voltage of 80 V using the Massey_optimized model for impact ionization.

7.5 Choice of E_C

In [2], it is stated that the value of the critical electric field for electrons in the Overstraeten deMan model is E_C =203 V µm^{-1}. This is actually the value for the critical electric field of holes [12]. For electrons it is 123 V µm^{-1} [12]. This parameter is used in the GainReduction function. To test that indeed, it should be E_C = 123 V µm^{-1}, the HPK-T3.1 is simulated at 80 V for both values of E_C in the GainReduction function in the accumulated gain algorithm. The result is shown in Figure 26. Indeed, the value should be 123 V µm^{-1}.

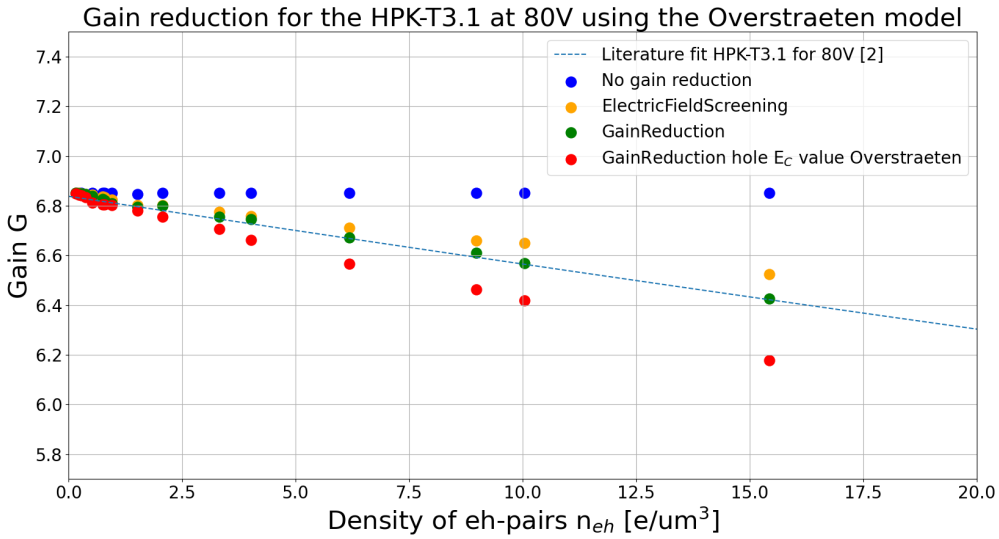

Figure 26: Simulation of the HPK-T3.1 at a bias voltage of 80 V using the Overstraeten model for impact ionization. In red, also the GainReduction function with the hole value for E_C is depicted.

7.6 Dependence on d_{gl}

In [2], an estimation of the gain layer thickness of both the HPK-T3.1 and the HPK-T3.2 is given. It is estimated that d_{gl} = 1.5 µm for the HPK-T3.1 and that d_{gl} = 2 µm for the HPK-T3.2. In [2], b and G_0 are obtained from data for the HPK-T3.1 and the HPK-T3.2. Using these parameters, we extract the value of d_{gl}. Then we get d_{gl} =1.5 µm for the HPK-T3.1 and d_{gl} =2.2 µm for the HPK-T3.2. Thus, the estimation of d_{gl} for the HPK-T3.2 is slightly off. A simulation of the HPK3.2 has been done for both d_{gl} =2 µm and for d_{gl} =2.2 µm. The results are shown in Figure 27. This shows that this correction on d_{gl} improves the accuracy of the GainReduction function. It also shows that the gain reduction is sensitive to the chosen value of d_{gl} thus careful thought should go into setting this value.

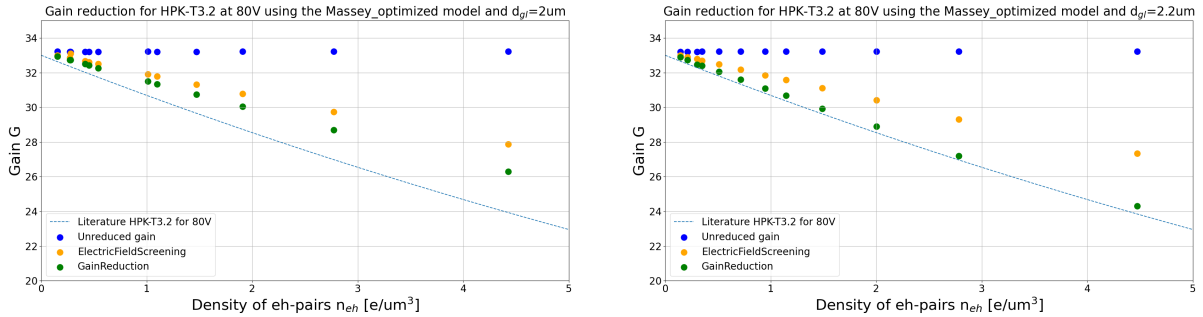

(a) $d_{\mathrm{gl}} = 2\,\mu\mathrm{m}$ (b) $d_{\mathrm{gl}} = 2.2\,\mu\mathrm{m}$

Figure 27: Simulation of the HPK-T3.2 at a bias voltage of 80 V using the Massey_optimized model for impact ionization. The simulation is done for the GainReduction and ElectricFieldScreening functions.

8 Measurement of the HPK2-W36

Aside from comparison to the measurements of two detectors also considered in [2], the implementation of gain reduction was also compared to measurements of the HPK2-W36 LGAD done at our group CERN-SSD. A TCAD simulation of the electric field of this LGAD is available [22]. The HPK2-W36 LGAD was chosen because it has a fairly low gain, which reduces the computation time of the simulation. The thickness is 54 µm and the unreduced gain is in the order of 10 at a bias voltage of 80 V. The TCAD simulation is one dimensional and the shape at 80 V is shown in Figure 28. An infrared laser at 1064 nm is used and the laser is injected from the top. In the next section, a brief description of the experimental method is given and in Section 8.2, the results of the measurements are compared to simulation.

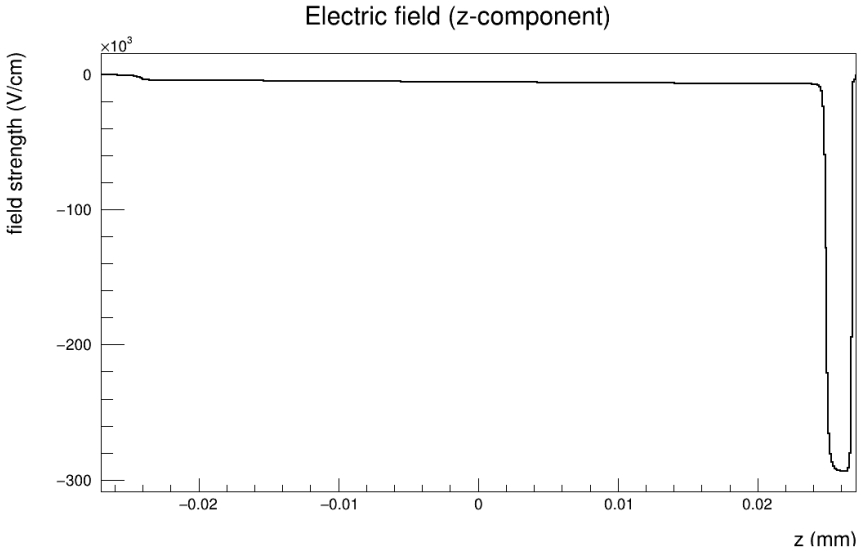

Figure 28: Electric field of the HPK2-W36 at 80 V from a TCAD (by Michael Moll).

8.1 Measurement method

The measurements are done in the Transient Current Technique (TCT) setup of the Solid State Detectors group at CERN [23]. A depiction of the coordinate system of the setup is given in Figure 29. In order to calculate the gain of the device, the charge of the LGAD is compared to the charge of the PIN. The PIN is a detector from the same wafer as the LGAD but without the gain layer. The density of charge carriers n_{eh} is varied in two ways. One way is by placing the detector in the focus point of the beam and varying the laser power. The other is by moving the detector in the z-direction such that it is not placed in the focus point of the beam and thus has an increased beam waist and thus a lower density. The measurement was done by undertaking the following steps.

First, we use the PIN to measure optical properties of the beam (beam waist, Rayleigh length and focal point). We need to make sure that the laser is fully injected into the detector by finding the position of the hole at the top. This hole is approximately 100x100 µm^2, thus to find it, a xy scan needs to be performed to find the position with maximum signal. Then, focus scan is performed to find the focus position. At each z, a knife edge scan is performed to obtain the beam waist. This means that an error function is fit over the signal as the detector moves in the x direction. The laser has a gaussian propagation, thus by fitting the beam waist at each z, we find the beam waist at the focus point, the z-position of the focus point and the Rayleigh length. The values obtained for the waist and Rayleigh length ar 4 µm and 180 µm respectively.

Next, we measure the signal of the PIN at the focus point. The output signal is the current induced by the movement of charge carriers. To convert this to a total induced charge Q_{ind}, we integrate the current over time. The induced charge of a PIN is independent of the z-position and the bias voltage, as long as the sensor is fully depleted. The total eh-pairs deposited in the sensor n_{eh} is calculated from the total induced charge Q_{ind} using $n_{\text{eh}} = \frac{Q_{\text{ind}}}{Be_0}$ where B is the amplification factor from the current amplifier. The volumetric density is then $\frac{n_{\text{eh}}}{\pi FWHM^2 d}$. This is repeated for several laser intensities to know the amount of deposited charge at various powers in the focus point. The density can be calculated using this total deposited charge and the known beam waist at each z.

Now we replace the PIN by the LGAD. For the power adjustment measurements, we keep the LGAD in the focus point and increase the power by decreasing the IR attentuator. For each power, we divide the induced charge of the LGAD by the induced charge of the PIN to obtain the gain. For the defocussing measurements, we move the LGAD away from the focus point in the z-direction with a constant power. Again, the gain is calculated at each z by dividing the induced charge of the LGAD by the induced charge of the PIN.

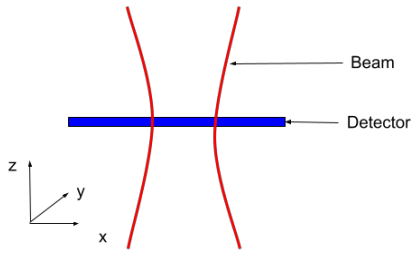

Figure 29: Setup including the definitions of the coordinates.

8.2 Results and analysis of experiment and simulation

The beam waist in the focus point was found to be 4 µm and its Rayleigh length 174 µm. Since the detector thickness is smaller than the Rayleigh length, the beam can be considered collimated inside the detector.

The results of the simulation as well as the measurements at a bias voltage of 80 V can be seen in Figure 30 including fits over the data. It can be observed that the simulated unreduced gain is not in agreement with measurements. The reason for this is unclear. For the measurements, the gain is approximately 10.5 whereas for the simulation, it is around 7.3. From TCAD simulations, one would expect a gain of 9.2. When the TCAD simulations are rerun but without the multiplication of holes, it results in a gain of 7.2. This gives an indication that the multiplication of holes might be relevant. However, whether the Allpix Squared simulation is run with or without hole multiplication, the gain remains 7.3, thus hole multiplication is not of significance in the Monte Carlo simulation. Why this is the case is not fully understood.

The predicted gain is 7.45, the average electric field is 240 kV cm^{-1} and b calculated by the simulation 0.004 73 µm^3. The fit over the GainReduction function shows approximately the same b value, which is as to be expected. As before, the ElectricFieldScreening function underestimates the reduction compared to the GainReduction function which corresponds to a smaller fitted b value. Because the unreduced gains deviate, it is difficult to conclude much on the accuracy of the simulation with this data. One thing we can see is that the fitted b value of the data is approximately the same as that of the GainReduction function. This is strange because the predicted gain is too low, thus we would expect b to be smaller. It could be because we chose d_{gl} too large, thus our average electric field is too low, but it is unclear if this is indeed the case. However, it is again clear that both measurement and simulation show the presence of the gain reduction phenomenon in the same order of magnitude.

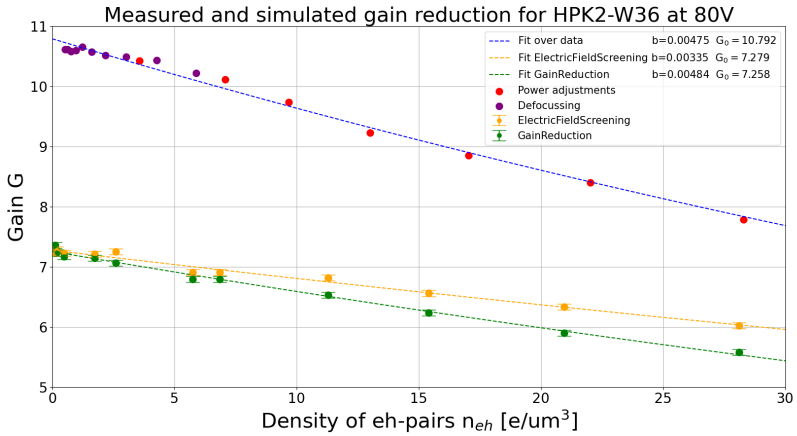

Figure 30: Simulation and measurement of the HPK2-W36 LGAD. The measurements for high gain are done by increasing the laser power and the measurements for low gain are done by defocussing the laser. The simulation is done for impact ionization model Massey_optimized and by assuming that d_{gl} =2.2 µm. A fit through the data is also shown.

9 Conclusion

In this thesis, the concept of gain reduction was implemented in the Allpix Squared simulation framework. This was done by adding three parts to the framework. First, an approximate electric field type describing the gain layer was added. It correctly implements the doping boxes approximation and obtains the right order of magnitude of the electric field when compared with TCAD simulations. The charge groups are accelerated in this field and a gain is obtained. It is known that the gain calculation is very sensitive to the thickness of the gain layer as well as the absolute value of the electric field, as can also be be deduced from Equation 1. Therefore, the size of the gap and the p^+-implant need to be estimated correctly to obtain a reasonable gain value. This estimation can be difficult when the exact shape of the gain layer is unknown, as is often the case.

The other two parts are two different functions simulating the gain reduction in two different ways. The compatibility with the results in [2] of the GainReduction and ElectricFieldScreening functions has been tested. The functions are also compared to our own measurements. The GainReduction function implements the approximation made in [2] well. Because the parameter b cannot be fit in the simulation but needs to be calculated, this can be a source of error. But if the correct thickness of the gain layer is set and the predicted gain is close to the gain of the detector, the reduction factor is calculated to a good accuracy. The ElectricFieldScreening function usually slightly underestimates the reduction compared to GainReduction and data. This is attributed to the fact that GainReduction assumes a constant electric field, which ElectricFieldScreening does not. GainReduction uses more assumptions than ElectricFieldScreening but manages to reproduce the results from [2] more accurately. When comparing the simulation to measurement, there is a discrepancy between the unreduced gain of the simulation and the measurement.

10 Discussion

There are several suggestions to further analyze the current implementation as well as improve upon it. Regarding the gain layer electric field type, it would be good to add the option to also include the n^{++}- and p^{++}-implant at the front and back of the detector. Regarding the gain reduction implementation, it would be good to verify some of the experiments done in this thesis with more charge carriers and secondary charge propagation turned on. Because of the computation time limitations, the probability based algorithm experiments could not be redone with more charges to see if the statistical fluctuations decrease.

As mentioned before, the predicted gain is calculated as the accumulated gain of an electron passing through the gain layer in N steps. Therefore its numerical value coincided with the unreduced gain given by the original accumulated gain algorithm. However, because the new probability based algorithm is implemented and simulations usually include hole multiplication and diffusion, it is important to reconsider if the calculation is still valid. For low gain it was observed that the predicted gain is very similar. For high gain, the difference was visible. Changing the calculation of the predicted gain to a probability based calculation would make it more compatible with the rest of the simulation framework, but it would also require more computation time, because it would require many trials.

Next, it is important to understand where the differences in gain between simulation and measurement originate. One possible reason could be the impact ionization coefficients, although the

coefficients have been optimized for these detectors by fitting a TCAD simulation to data. It should also be investigated if the gain of the simulation differs from measurement because of the assumption that holes do not multiply in Allpix Squared. Aside from the difference between simulation and measurement, more investigation is also needed on the difference between the accumulated gain algorithm and the probability based algorithm.

The following improvements should be made to the gain reduction functions. First, there should be models added that calculate the density in a different way and therefore allow for more deposition types. For now, it only works for an IR laser with no gaussian propagation, but it would be good to also allow for depositions from for example inclined particle tracks. Secondly, the parametrization on which the implementation is based is a first order approximation. From the results of this parametrization in [2], there is room to improve the correspondence between data and fit. The implementation could be improved by adding a time dependence to include diffusion and considering a non-uniform density distribution and thus for example making ΔE both space and time dependent. This might however be quite difficult to do without considerably increasing the computation power needed. Inspiration for other ways to parametrize gain reduction can for example be found in [24].

Acknowledgements

I would like to thank Marcos Fernandez from CERN for his excellent supervision over this project and all his help working with such a simulation framework in Linux, but also for his work on measuring our own device. It was a pleasure to share an office and a laugh with you.

I would like to thank Frank Filthaut from Radboud University for the supervision and all of his help in getting me this internship. I know it was a lot of work to organize it and I really appreciate all the time and effort.

I would like to thank Michael Moll for taking me in as an intern in the group and for his supervising role and all the help with the TCAD simulation.

I would like to thank the entire SSD group for their openness for new arrivals in the group and all the spontaneous chats over coffee and 3D printing.

I would like to thank the maintainers of Allpix Squared, in particular Simon Spannagel and Paul Schütze, for their help with my Allpix Squared questions.

I would like to thank the HGTD group at CERN as well as Nikhef and the High Energy Physics department at Radboud University for their (financial) contributions to make this internship possible.

Last, but definitely not least, I would like to thank my father and mother and my boyfriend Max for having the patience to listen to me talk about the internship for months.

References

[1] S. Spannagel, K. Wolters, D. Hynds, N. Alipour Tehrani, M. Benoit, D. Dannheim, N. Gauvin, A. Nürnberg, P. Schütze, and M. Vicente. Allpix2: A modular simulation framework for silicon detectors. *Nuclear Instruments and Methods in Physics Research Section A: Accelerators, Spectrometers, Detectors and Associated Equipment*, 901:164–172, 2018.

[2] G. Kramberger, B. Hiti, V. Cindro, A. Howard, I. Mandić, M. Mikuž, M. Petek, A. Ristić, and G. Ristić. Gain dependence on free carrier concentration in lgads. *Nuclear Instruments and Methods in Physics Research Section A: Accelerators, Spectrometers, Detectors and Associated Equipment*, 1046:167669, 2023.

[3] Alice. Available at `https://home.cern/science/experiments/alice`.

[4] Lhcb. Available at `https://home.cern/science/experiments/lhcb`.

[5] Atlas. Available at `https://atlas.cern/Discover/Detector`.

[6] Cms. Available at `https://cms.cern/detector`.

[7] S.M. Sze. *Semiconductor Devices: Physics and Technology*. John Wiley & Sons Singapore Pte. Limited, 2012.

[8] P. Hofmann. *Solid State Physics: An Introduction*. Wiley, 2015.

[9] Forward and reverse bias. Available at `http://hyperphysics.phy-astr.gsu.edu/hbase/Solids/diod.html`.

[10] M. Ferrero, R. Arcidiacono, and M. Mandurrino. *Ultra-fast Silicon Detectors: Design, Tests, and Performances*. Series in sensors. CRC Press, 2021.

[11] A. G. Chynoweth. Ionization rates for electrons and holes in silicon. *Phys. Rev.*, 109:1537–1540, Mar 1958.

[12] R Van Overstraeten and H De Man. Measurement of the ionization rates in diffused silicon pn junctions. *Solid-State Electronics*, 13(5):583–608, 1970.

[13] E. Currás, M. Fernández, and M. Moll. Gain reduction mechanism observed in low gain avalanche diodes. *Nuclear Instruments and Methods in Physics Research Section A: Accelerators, Spectrometers, Detectors and Associated Equipment*, 1031:166530, 2022.

[14] S. Agostinelli et al. Geant4—a simulation toolkit. *Nuclear Instruments and Methods in Physics Research Section A: Accelerators, Spectrometers, Detectors and Associated Equipment*, 506(3):250–303, 2003.

[15] Root - an object oriented data analysis framework, 1997.

[16] Gaël Guennebaud, Benoît Jacob, et al. Eigen v3. http://eigen.tuxfamily.org, 2010.

[17] S. Ramo. Currents induced by electron motion. *Proceedings of the IRE*, 27(9):584–585, 1939.

[18] Mathieu Benoit. Pixel detector r&d for the compact linear collider, Feb 2019.

[19] C. Jacoboni and C. Canali et al. A review of some charge transport properties of silicon. *Solid-State Electronics*, 20(2):77–89, 1977.

[20] C. Scharf and R. Klanner. Measurement of the drift velocities of electrons and holes in high-ohmic ⟨100⟩ silicon. *Nuclear Instruments and Methods in Physics Research Section A: Accelerators, Spectrometers, Detectors and Associated Equipment*, 799:81–89, 2015.

[21] D.J. Massey, J.P.R. David, and G.J. Rees. Temperature dependence of impact ionization in submicrometer silicon devices. *Electron Devices, IEEE Transactions on*, 53:2328 – 2334, Oct 2006.

[22] Michael Moll. Cv/iv characteristics of lgads, Oct 2021.

[23] Tct-setup at cern-ssd. `https://indico.desy.de/event/12934/`.

[24] H. Raether. *Electron Avalanches and Breakdown in Gases*. Butterworths advanced physics series. Butterworths, 1964.

[25] L Devroye. *Non-Uniform Random Variate Generation*. Springer, Nov 2013.

Appendix

A The code and the Gitlab repository

The implementation can be found in `https://gitlab.cern.ch/fdewit/allpix-squared` and in `https://gitlab.cern.ch/SSD/allpix-squared-gain-reduction`. The branch containing the old accumulated gain algorithm is the "gain_reduction" branch. The branch with the new probability based algorithm is called "gain_reduction_prob_based". In both branches, GainReduction and ElectricFieldScreening can be found under `allpix-squared/src/physics` and are called `GainReduction.hpp` and `ElectricFieldScreening.hpp`. They can be included into any propagation module in the following way. In the initializer, they are prepared using

```
gain_reduction_ = GainReduction(config_,detector_)
```

and

```
electric_field_screening_ = ElectricFieldScreening(config_,detector_).
```

At the start of the run part, the density is calculated as

```
gain_reduction_.setDensity(deposits_message->getData())
```

and

```
electric_field_screening_.setDensity(deposits_message->getData()).
```

Then, the functions are applied in the propagate part by reducing the electric field from which the multiplication is determined by

```
electric_field_screening_(static_cast<ROOT::Math::XYZPoint>(position))
```

and after that reducing the local_gain by a factor

```
gain_reduction_(local_gain,static_cast<ROOT::Math::XYZPoint>(position)).
```

The implementation of the gain layer electric field type can be found in the file `allpix-squared/src/modules/ElectricFieldReader/ElectricFieldReaderModule.cpp`. Each branch also contains a file called `examples/experiments_thesis_femke` which contains the relevant configuration files used in Section 6 and 7. However, one should be mindful that the settings in the propagation module can be different for some experiments, such as turning off diffusion and propagation of secondary charges and adjusting histogram sizes.

B Inversion method

In the probability based algorithm, the amount of secondaries calculated in a single step for a single charge carrier is calculated by drawing randomly from a geometric distribution. The geometric distribution is described by the probability function $\mathcal{P}(N = n) = (1-p)^{n-1}p$ for a stochastic variable N and with parameter p. The mean μ of this distribution is $\mu = \frac{1}{p}$. In the probability based algorithm, the mean is fixed by the local gain and is set to be $\mu = G_{\text{local}} = \frac{1}{p}$. Thus, $p = \frac{1}{G_{\text{local}}}$. To draw randomly from this distribution, the inversion method is used on the right

distribution function $\mathcal{P}(N > n)$. This inversion method entails that the inverse of the function $\mathcal{P}(N > n) = u$ is used to draw a random n from the geometric distribution using a random draw u from the uniform distribution. n is for the moment taken to be real [25]. For the geometric distribution with $p = \frac{1}{G_{\text{local}}}$, $\mathcal{P}(N > n) = (1 - \frac{1}{G_{\text{local}}})^n$. From inverting this, the result is obtained as

$$n = \log_{(1-\frac{1}{G_{\text{local}}})}(u) = \frac{\ln(u)}{\ln(1 - \frac{1}{G_{\text{local}}})}. \tag{35}$$

Drawing a random sample from the uniform distribution and applying this function is equivalent to drawing a random sample from the geometric distribution. This is because $n \to \mathcal{P}(N > n)$ is by definition monotone decreasing from 1 to 0, thus injective, and surjective on $[0, 1]$. Taking a random sample from the image and finding the inverse, is effectively the same as drawing a random sample from the geometric distribution. n can now be floored to obtain integer gain.

C Results of the simulations of the HPK-T3.1 and HPK-T3.2

The following part displays the results of all the simulations performed for this thesis. Part of these results are also displayed in the results and analysis of the HPK-T3.1 and HPK-T3.2.

Figure 31 displays the results of simulations on the HPK-T3.1 in the accumulated gain algorithm. It shows the results for bias voltage 80 V in Figure 31a and for bias voltage 70 V in Figure 31b. Each shows the results for both the Massey model and the Overstraeten model for impact ionization. The unreduced gain, ElectricFieldScreening, GainReduction and GainReduction with the hole value for E_C are depicted.

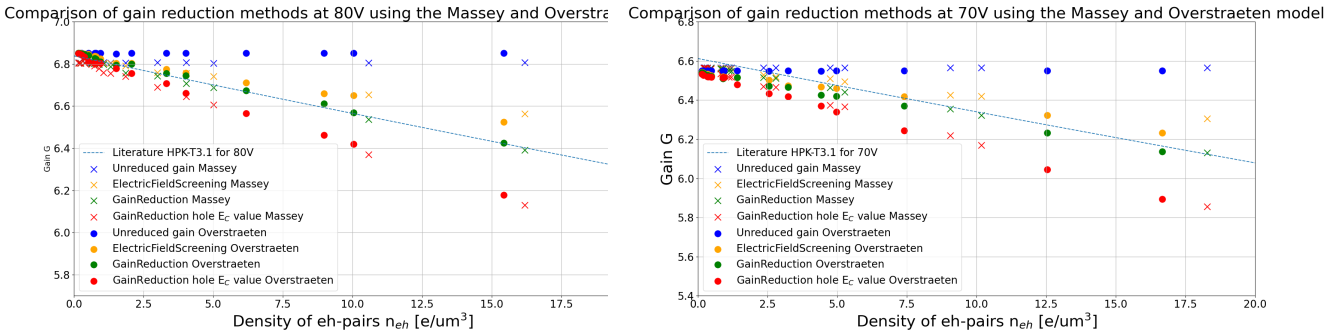

(a) 80 V (b) 70 V

Figure 31: Simulation of the HPK-T3.1. d_{gl} is assumed to be 1.5 µm for GainReduction and ElectricFieldScreening functions. The plots display the final gain of the primary electrons after propagation for various methods of gain reduction for the HPK-T3.1 under 80 V and 70 V bias voltage and using the Massey and Overstraeten model for the impact ionization compared to the fit function from [2].

Figure 32 displays the results of simulations on the HPK-T3.2 in the accumulated gain algorithm. In these simulations, d_{gl} =2 µm is used for the gain reduction functions. It shows the results for bias voltage 80 V in Figure 32a and for bias voltage 90 V in Figure 32b. The Massey_optimized model is used. The unreduced gain, ElectricFieldScreening, GainReduction and GainReduction with the hole value for E_C are depicted.

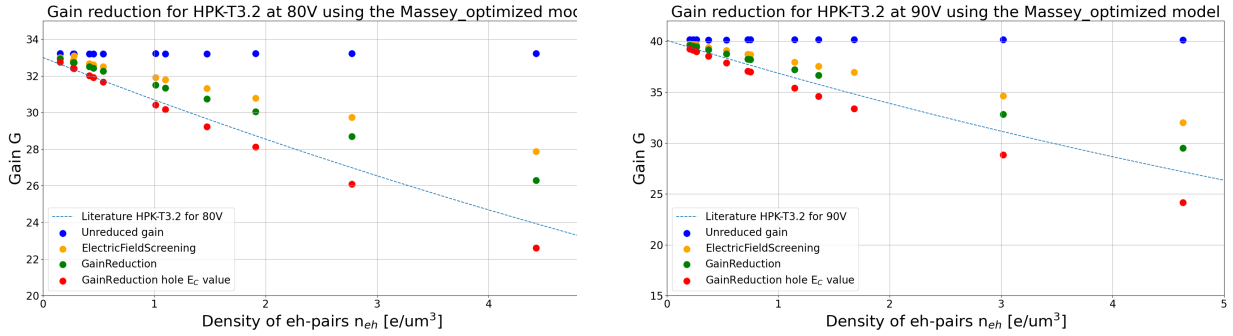

(a) 80 V (b) 90 V

Figure 32: Simulation of the HPK-T3.2. d_{gl} is assumed to be 2 µm for GainReduction and ElectricFieldScreening functions. The plots display the final gain of the primary electrons after propagation for various methods of gain reduction for the HPK-T3.2 under 80 V and 90 V bias voltage and using the Massey_optimized model for the impact ionization compared to the fit function from [2].

Figure 33 displays the results of simulations on the HPK-T3.2 in the accumulated gain algorithm. In these simulations, d_{gl} =2.2 µm is used for the gain reduction functions. It shows the results for bias voltage 80 V in Figure 33a and for bias voltage 90 V in Figure 33b. The Massey_optimized model is used. The unreduced gain, ElectricFieldScreening, GainReduction and GainReduction with the hole value for E_{C} are depicted.

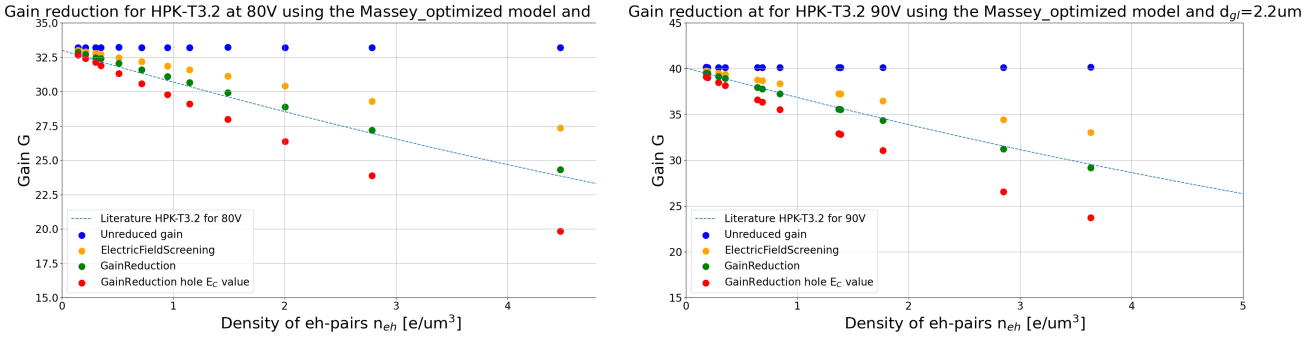

(a) 80 V (b) 90 V

Figure 33: Simulation of the HPK-T3.2. d_{gl} is assumed to be 2.2 µm for GainReduction and ElectricFieldScreening functions. The plots display the final gain of the primary electrons after propagation for various methods of gain reduction for the HPK-T3.2 under 80 V and 90 V bias voltage and using the Massey_optimized model for the impact ionization compared to the fit function from [2].

Figure 34 displays the results of simulations on the HPK-T3.1 in the probability based algorithm. The bias voltage is 80 V. It shows the results for the Massey model in Figure 34a and the Overstraeten model in Figure 32b. The ElectricFieldScreening and GainReduction function are depicted.

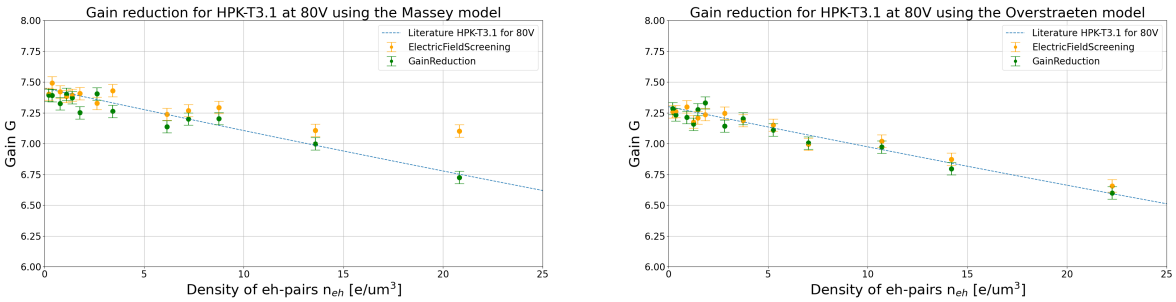

(a) Massey (b) Overstraeten

Figure 34: Simulation of the HPK-T3.1 at 80 V using the probability based algorithm. The same configuration is used as for the accumulated gain algorithm. The simulation is done for impact ionization models Massey and Overstraeten. The results from [2] corrected for the dissimilar unreduced gain is shown as a blue dashed line.

Figure 35 displays the results of simulations on the HPK-T3.1 in the probability based algorithm. The bias voltage is 70 V. It shows the results for the Massey model in Figure 35a and the Overstraeten model in Figure 35b. The ElectricFieldScreening and GainReduction function are depicted.

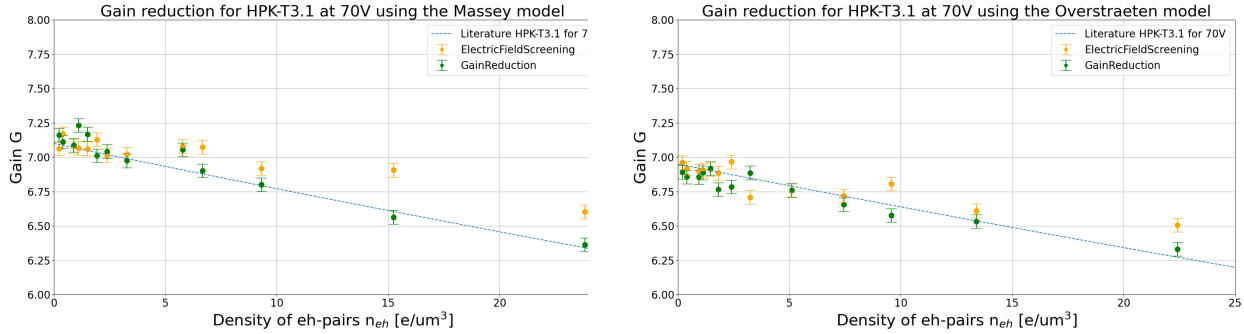

(a) Massey (b) Overstraeten

Figure 35: Simulation of the HPK-T3.1 at 70 V using the probability based algorithm. The same configuration is used as for the accumulated gain algorithm. The simulation is done for impact ionization models Massey and Overstraeten. The results from [2] corrected for the dissimilar unreduced gain is shown as a blue dashed line.

Figure 36 displays the results of simulations on the HPK-T3.2 in the probability based algorithm. It shows the results for bias voltage 80 V in Figure 35a and for bias voltage 90 V in Figure 35b. The Massey_optimized model is used. The ElectricFieldScreening and GainReduction function are depicted.

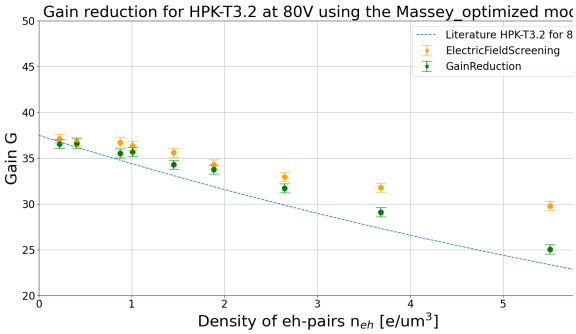

(a) 80 V

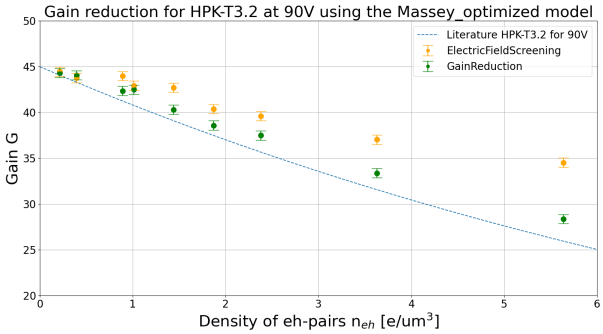

(b) 90 V

Figure 36: Simulation of the HPK-T3.2 at 80 V and 90 V using the probability based algorithm. The same configuration is used as for the accumulated gain algorithm. The simulation is done for impact ionization model Massey_optimized. The results from [2] corrected for the dissimilar unreduced gain is shown as a blue dashed line.